A Synthesis of a Rabbit Ventricular Myocyte Model Based on a Chudin Formulation of Calcium Dynamics (Computer Simulation Study)

CSD-TR050035

R. Samade and B. Kogan

August 2005

A Synthesis of a Rabbit Ventricular Myocyte Model Based on a Chudin Formulation of Calcium Dynamics (Computer Simulation Study)

R. Samade[†] and B. Kogan[‡]
[†]Biomedical Engineering Department and [‡]Computer Science Department,
University of California, Los Angeles, California, USA.

1. Abstract

The formulation of the first Luo-Rudy guinea pig ventricular myocyte (LR-I) model provided one of the first detailed mathematical ionic models of cardiac action potential (AP) and currents. After an extensive reformulation of sodium and potassium ionic dynamics and the introduction of calcium (Ca^{2+}) dynamics, Luo and Rudy presented one of the first of a second generation of AP models, the dynamic Luo-Rudy model (LRd). With those modifications, a new model became available for use in computer simulations that takes into account the role of intracellular calcium ($[Ca^{2+}]_i$) dynamics on AP generation and propagation through cardiac tissue. Modifications of $[Ca^{2+}]_i$ dynamics to the LRd model was done by Chudin et al. Other researchers, such as Bers, Puglisi, McCullough, and Shiferaw used the baseline formulation of the LRd model to develop models of rabbit ventricular myocytes. These events have occurred at the same time that physiological experiments in the frame of recent projects are supposed to utilize rabbit hearts. Therefore, to compare simulation results with physiological experiments, the model of the rabbit ventricular myocyte, with $[Ca^{2+}]_i$ dynamics, is extremely important.

The comparisons of the models occurred under both low and high pacing rate regimes, first with the comparison of guinea pig and rabbit formulations of sodium and potassium dynamics, both containing LRd $[Ca^{2+}]_i$ dynamics. Then with the addition of Chudin and Shiferaw $[Ca^{2+}]_i$ dynamics to the rabbit model version of sodium and potassium dynamics, low and high pacing rate comparisons were conducted, with and without the inclusion of Ca^{2+} spontaneous release. Under baseline model conditions, $[Ca^{2+}]_i$ alternans (alternating amplitude) as well as DADs were observed in the rabbit version of the LRd model, but not in the guinea pig version. Alternans was observed in the Shiferaw based model after a long period of high rate stimulation, but the modified Chudin rabbit model showed alternans-like behavior much earlier. The appearance of alternans-like behavior in the Shiferaw model of $[Ca^{2+}]_i$ was dependent mainly on Ca^{2+} efflux processes, such as the sodium-calcium exchanger and the sarcolemmal pump. With higher rates of stimulation, $[Ca^{2+}]_i$ alternans behavior in the modified Chudin model was accompanied by greater Ca^{2+} release into the myoplasm from spontaneous calcium release, in conjunction with a decrease in the sodium-calcium exchanger.

2. Introduction

Previous investigations of various types of pathological phenomena, such as ventricular tachycardia (VT) and ventricular fibrillation (VF), performed in computer simulations have been based on the original Luo-Rudy (LR-I) model [1] and its further development [2,3] and modification [2,4]. These are all mathematical ionic models of ventricular guinea pig myocytes and, in their most general considerations, have been suitable for many simulation purposes. Recent physiological experiments [5,6,7,8,9] have used rabbit subjects (usually New Zealand white rabbits) extensively. Due to this, our modeling of the ventricular myocyte AP requires us to synthesize and use a model based on the rabbit instead of guinea pig species.

With the usage of rabbits in more physiological experiments investigating cardiac arrhythmias, several researchers have developed mathematical ionic models that can appropriately model the electrophysiology particular to the rabbit species. One of the most widespread rabbit models is LabHEART [7], a version of the LRd model modified to model accurately the rabbit ventricular myocyte. Another formulation proposed for modeling a dynamical rabbit ventricular myocyte model, specifically calcium (Ca^{2+}) dynamics, is the one proposed by Shiferaw et al [4], which introduces multiple compartments in the cytosolic region outside of the sarcoplasmic reticulum (SR). By modeling Ca^{2+} dynamics in this manner, the Shiferaw model takes into account graded release due to the recruitment of local Ca^{2+} release events (Ca^{2+} sparks) [4,10,11,12].

The Shiferaw and LabHEART models are both based on the Hodgkin-Huxley (H-H) formulation [13], but in the case of [7] introduced parameters that modeled rabbit myocyte sodium and potassium dynamics while incorporating, with small changes, the Ca^{2+} dynamics formulated in the LRd model. In [4], the sodium and potassium dynamics are modeled the same as in [7], but with significant changes in Ca^{2+} dynamics.
The LabHEART model, with respect to Ca^{2+} dynamics, has the same drawbacks as the LRd model, such as a discrete, rather than continuous description of the Ca^{2+}-induced, Ca^{2+}-release (CICR) process and non-accurate modeling of physiological data obtained at high pacing rates. As for the Shiferaw model, its Ca^{2+} dynamics have no spontaneous release, alternans of Ca^{2+} dynamics appears during fast pacing with a comparatively low concentration of $[Ca^{2+}]_i$, and its morphology changes significantly with time.

Therefore, we decided to consider the possibility of improving the Chudin model for a better representation of the rabbit myocyte and to avoid the disadvantages of the formulations in both of the above models. In this paper, we seek to synthesize a new mathematical ionic model for the rabbit ventricular myocyte for future use in multi-dimensional experiments modeling cardiac tissue in the rabbit heart. By achieving this aim, we wish to implement computer simulations that can accurately model the rabbit ventricular myocyte, compared to physiological experiments, and allow for the study of physiological and pathophysiological behavior, such as ventricular tachycardia (VT) and ventricular fibrillation (VF).

3. Modeled Action Potential Dynamics of the Rabbit Myocyte and its Distinctions from the Myocyte of the Guinea Pig

The formulation of a reliable mathematical ionic model of the AP in a rabbit ventricular myocyte for usage in modeling cardiac tissue requires a close examination of key characteristics observed in physiological experiments with rabbit test subjects. This process, similar to that done for the LRd guinea pig ventricular myocyte model, was done by several researchers [4,7] and was based on available experimental data from physiological experiments. These models share a common basis for their formulation, the LRd model, but are modified to reflect rabbit ventricular myocytes. It should be noted that the characteristics of the the models, while both derived from the LRd model, are distinguished by differences in their formulations of $[Ca^{2+}]_i$. In addition, there is increased amplitude for the I_{NaCa} exchanger in addition to different formulations for I_{cicr} and I_{spon} in the rabbit model. Other than these differences, it appears there are relatively few differences in the equations that represent the rabbit myocyte, so the question naturally arises of why a new model is necessary. It is the aim of this section to illustrate the differences in mathematical expressions and morphologies between models representing APs of guinea pig and rabbit myocytes. With this goal in mind, the differences between the two models will provide a justification for choosing and modifying a mathematical ionic model representative of the characteristics of the rabbit myocyte.

3.1. Membrane Currents and Electrophysiological Parameters

The models chosen for the basis of the comparison of species-specific models are the LRd model to represent the guinea pig ventricular myocyte and the Puglisi-Bers model (derived from LabHEART) to represent the rabbit ventricular myocyte. The first step of the investigation of the differences between models of the two species involves analysis of the differences in their underlying mathematical expressions. This was done using the results from Puglisi [7] and work by Van [14] to formulate the rabbit model.

3.2. Initial Conditions for Model State Variables

Initial conditions for the system of partial differential equations in all models were determined by pacing each of the models at a BCL = 1500 ms for 5 beats and allowing their respective computer simulations to run for 5 additional seconds past the time of the last applied stimulus. This allowed enough time for the state variables of the model to come to their steady-state values, which established the set of initial conditions for the model. These initial conditions were then used for the models when subsequent simulation experiments were performed. The same procedure was used with the modified Chudin and Shiferaw models described in the next section and the values for their initial conditions are presented in Part I and Part II, respectively, of the Appendix. For all experiments, simulations were performed on a workstation PC with a 1.60 GHz Intel processor. The time step algorithm used for simulations was a variable time step (VTS) algorithm, where the time step used for the integration of the system of model equations assumed values of either 0.005 ms or 0.1 ms, depending on the magnitude of the change

of the AP ($\frac{dV}{dt}$). In this algorithm, the smaller time step is used for larger $\frac{dV}{dt}$ and the converse for the larger time step. The details of this algorithm are outlined in [15]

3.3. Ionic Current and Action Potential Morphologies at Low Pacing Rates

The results of the simulations of the APs are show in Figure 1. This figure compares morphologies of the APs given by mathematical models for the guinea pig and rabbit myocytes in two frames of time, with a BCL = 1500 ms. In panel A, the full time course of the APs for both models can be seen, with the AP of the guinea pig representation having a peak V_{max} 16% larger than that of the rabbit AP. The AP produced by the rabbit model, however, showed an approximately 19 ms lengthening of APD_{90} over the guinea pig representation. Panel B presents a magnified view of phase 0 of both APs, showing that both have nearly identical rise times (the discrepancy due to the different time courses of the fast sodium current) , but with different V_{max} values.

Comparisons of currents are provided in the content of Figure 2. The six plots given shows the morphologies of the main currents affecting the APs and vice versa of both models, paced at BCL = 1500 ms. The top plot of panel A shows that while both models have similar time courses for the fast sodium current, the rabbit model has a 47% smaller current. In the middle plot of panel A, the sodium-calcium exchanger currents in both models are very similar, with the rabbit model showing a longer net outward current (a prolongation of 25 ms). Calcium currents are compared in the bottom plot of panel A, showing a larger magnitude in both the L-type calcium current and the sarcolemmal calcium pump in the rabbit model as opposed to the guinea pig model. Panel B's top plot gives a comparison of the potassium currents in both models, with the fast delayed rectifier currents having similar morphologies with an ~25 ms delay in the rabbit model. The slow delayed rectifier currents, however, of both models diverge from each other, with the guinea pig model having a significantly higher magnitude. A comparison of the non-specific potassium and sodium currents is presented in the middle plot of panel B, showing a larger potassium and sodium component in the rabbit model as compared to the guinea pig model. New currents introduced in the rabbit model, the transient outward current and the calcium-activated chorine current, are shown in the bottom plot of panel B, which result in the sharp repolarization seen in early Phase 1.

3.4. Ionic Current and Action Potential Morphologies at High Pacing Rates

In order to fully understand the effects of what introducing rabbit sodium and potassium dynamics would have to models with Chudin and Shiferaw formulations of $[Ca^{2+}]_i$ dynamics, it was necessary to study both the guinea pig and rabbit models in the high pacing rate regime. The effect of high pacing rate on AP and $[Ca^{2+}]_i$ is shown in Figure 3, where time courses of AP and intracellular calcium in the rabbit and guinea pig mathematical models are given for BCL = 150 ms. The pacing protocol for both models involved pacing with five initial beats longer than 150 ms in duration, which progressively shortened from 250 ms to 150 ms. This procedure was carried out in order to insure that APs in both models would shorten enough in APD_{90} due to dynamic

restitution to allow for stationary AP behavior with respect to time. After about 1 s of pacing, periodic alternans of intracellular calcium amplitude arises in the rabbit model, with large peaks corresponding to shortened APDs and vice versa. The guinea pig model, however, exhibits steady accumulation of intracellular calcium without alternans for the first 4.4 seconds of pacing. After this time period, two large releases of calcium from the JSR to the myoplasm due to spontaneous calcium release are observed, followed by the termination of the pacing protocol with the 30^{th} beat. While the guinea pig model recovers from its systolic peak to return toward its resting state concentration, the rabbit model exhibits a spontaneous rise of systolic calcium at 5.3 s into the simulation, corresponding to a delayed after-depolarization (DAD) in the AP (indicated by the downward arrows).

As for the currents during the time frame of the voltage and calcium described above, they are illustrated in Figure 4, which gives comparisons of currents produced by the guinea pig and rabbit models at high pacing rates (BCL = 150 ms). The six plots given show the effects of fast stimulation rates on several currents in the two models, with all currents measured in the 30^{th} and final beat. The top plot of panel A displays traces for the fast sodium current for the models, with the current in the rabbit model having decreased faster than the one in the guinea pig model. In the middle plot of panel A, the difference in the durations of the outward current phase of the sodium-calcium exchanger between both models has largely disappeared. The plot of calcium currents, shown in the bottom plot of panel A, shows a reduction of discrepancies in magnitudes of the L-type calcium currents in both models and nearly identical traces of the sarcolemmal calcium pump. In Panel B's top plot, a comparison of the potassium currents in both models is given and it can be seen that there is almost a complete disappearance of the discrepancy in time delay of the rapid delayed rectifier current that was seen at slow pacing rates. Also, the slow delayed rectifier current (similar to the rapid delayed rectifier current) shows a shorter time to peak due to dynamic AP restitution at high pacing rates, with a rapid increase at the onset of stimulus application and a smaller difference in current magnitudes midway between their values during low pacing rates. Non-specific potassium and sodium currents are compared in the middle plot of panel B, showing that the amplitudes of both the sodium and potassium currents in both models have increased, with both types of currents larger in the guinea pig model (a reversal of the situation in the low pacing rate regime). The bottom plot of panel B, showing the transient outward potassium and calcium-activated chlorine currents, illustrate little change in the amplitude and time course of the calcium-activated chlorine current, but a 40% decrease in the peak of the transient outward current.

4. Comparison of Calcium Dynamics in Shiferaw and Chudin Models

With the differences between the results of AP models of guinea pig and rabbit myocytes made apparent in the previous section, it becomes clear that in order to accurately model physiological data obtained from rabbit test subjects, an AP model based on their unique physiological characteristics must be synthesized and used. To accomplish this goal, two models were constructed and used as the basis for comparisons to ascertain which would be a more suitable model. The first is referred to here as the

modified Chudin model, which is the model of the guinea pig AP developed by Chudin, but incorporating features from the rabbit model given in [7]. The second is labeled as the Shiferaw model, which is a rabbit AP model based on the calcium cycling equations formulated in [4]. By comparing these two models under conditions of low and high pacing rates, more accurate discrimination between the two models can be made and the one can be chosen, which better suits to our modeling and computer simulation tasks. A summary of the changes to the model necessary to implement the modified Chudin model is given in Table 1 and equations for both models are listed in the Appendix.

4.1. Model Formulation with Chudin Calcium Dynamics

The formulation of the modified Chudin mathematical model for the rabbit ventricular myocyte was done using information from [2,7,16]. A complete description of the resulting model is given in Part I of the Appendix.

4.2. Model Formulation with Shiferaw Calcium Dynamics

In a similar manner to the modified Chudin mathematical model for the rabbit ventricular myocyte, the Shiferaw model used information from [2,4,16]. A complete description of the resulting model is given in Part II of the Appendix. A key characteristic of the Shiferaw model is the release function *Q*, which determines the amount of calcium released from the sarcoplasmic reticulum (SR) network. Its dependence on the JSR calcium concentration ($[Ca^{2+}]_{jsr}$) is plotted in Figure 5 and it is mentioned here in order to note its importance in controlling CICR and hence $[Ca^{2+}]_i$ dynamics.

4.3. Results Using Low Rates of Stimulations

Simulated ventricular APs in the modified Chudin and Shiferaw rabbit myocyte models are shown in Figure 6. It should be noted that in order to make a comparison solely of the effects of combining Chudin or Shiferaw intracellular calcium dynamics with the sodium and potassium dynamics of the Puglisi-Bers model, a few modifications to the baseline modified Chudin and Shiferaw models were made. These changes include the deactivation of spontaneous release in the modified Chudin model (so that both models have no spontaneous release), setting the coefficient $k_{NaCa} = 1177\ \mu A/cm^2$ in both models, and implementing the sarcolemmal pump in both models. Figures 6-9 exhibit the results of the experiments with these changes. In Figure 6, a comparison of the morphologies of the APs given by mathematical models for the Chudin and Shiferaw rabbit myocytes in two frames of time, with a BCL = 1500 ms is presented. In panel A, the full time course of the APs for both models can be seen, with the APs of both models having nearly identical V_{max} values. The AP produced by the Chudin model, however, showed a more than 40 ms longer APD_{90} than the Shiferaw model. Panel B presents a magnified view of phase 0 of both APs, showing that both have nearly identical rise times and V_{max} values.

Comparisons of currents are given in Figure 7. The six plots given shows the morphologies of the main currents affecting the APs and vice versa for both rabbit

models, paced at BCL = 1500 ms. The top plot of panel A displays traces for the fast sodium current for the models, both nearly identical to each other. In the middle plot of panel A, the morphologies differ between the two models, with a larger net outward current in the Shiferaw model. Calcium currents are compared in the bottom plot of panel A, showing a nearly four fold increase of L-type calcium current in the Shiferaw model over the Chudin model. The sarcolemmal pump was not actually included in the Shiferaw model, but its trace is shown for completeness. Panel B's top plot gives a comparison of the potassium currents in both models, with the fast delayed rectifier currents having similar morphologies, but different time courses for both models. The slow delayed rectifier currents, however, of both models diverge from each other, with the Chudin model having a significantly higher magnitude. A comparison of the non-specific potassium and sodium currents is presented in the middle plot of panel B, showing that the Shiferaw model has much greater potassium and sodium components in terms of current amplitude. The bottom panel of B displays comparisons of the transient outward potassium and calcium-activated chlorine currents, with the two models having nearly identical transient outward potassium currents, but a divergence in the morphologies of the calcium-activated chlorine currents.

4.4. The Effect of Higher Pacing Rates on Electrophysiological Phenomena

As in the case of the comparison between the guinea pig and rabbit models, it was necessary to investigate the effect of high pacing rate on the ionic dynamics of the Chudin and Shiferaw $[Ca^{2+}]_i$ models. The AP and $[Ca^{2+}]_i$ are shown in Figure 8, conducted with the same experimental protocol as done for the data shown in Figure 3. For BCL = 150 ms, a main feature of the behavior of both models in the high pacing rate regime is that the significant difference in APD_{90} disappears as the dynamic AP restitution properties of both cells shortens the APDs in response to the rate of stimulation. Unlike the case of the guinea pig and rabbit comparison, no alternans in APD is evident in either model. For the plot of intracellular calcium in both models during the same time period, a much higher level of systolic calcium is reached with each successive beat in the modified Chudin model compared to the Shiferaw model. However, no calcium amplitude alternans nor DADs after the cessation of pacing is present in either model in contrast to the presence of both phenomena in the Puglisi-Bers rabbit model.

With Figure 9, the six plots show the morphologies of the main currents affecting the APs for both rabbit models, paced at BCL = 150 ms and with all measurements taken at the 30^{th} beat. The top plot of panel A displays traces for the fast sodium current for the models, with the current in the Chudin model nearly zero in contrast to the still significant current from the Shiferaw model. In the middle plot of panel A, there is a larger net outward in the Shiferaw model, but the differences between the models are less acute than in the case of low pacing rates. Calcium currents are compared in the bottom plot of panel A, showing a greatly reduced discrepancy in magnitudes of the L-type calcium currents in both models. As for the sarcolemmal pump its traces in both models are nearly concise with each other as well. Panel B's top plot gives a comparison of the potassium currents in both models, with a decrease in the differences of the time courses of the fast delayed rectifier currents in both models compared to low pacing rates. The slow delayed rectifier currents, however, still differ greatly in magnitude, with the

Chudin model being significantly larger in magnitude than the Shiferaw model at high and low pacing rates. A comparison of the non-specific potassium and sodium currents is presented in the middle plot of panel B, showing that the Shiferaw model has greater potassium and sodium components in terms of current amplitude in high as well as low pacing rates, but less accentuated than at low pacing rates. The bottom panel of B displays comparisons of the transient outward potassium and calcium-activated chlorine currents, with a noticeable decrease in the transient outward current in the Chudin model, but no difference in the calcium-activated chlorine current.

4.5. The Sarcolemmal Pump and the Sodium Calcium Exchanger in the Shiferaw Calcium Model

From the high pacing rate experiments with the Shiferaw model of intracellular calcium dynamics, no alternans was observed. The appearance of calcium alternans is closely correlated to the accumulation of intracellular calcium and the instability of the calcium cycle that results from it and therefore it became necessary to examine key calcium membrane currents, such as the sarcolemmal pump and the sodium-calcium exchanger. The task of investigating the effect of depressing these two currents is accomplished by the experiments illustrated in Figure 10. The three plots shown demonstrate the effect of either decreasing the strength of the sodium-calcium exchanger (by decreasing k_{NaCa}), disabling the sarcolemma pump (as was the original condition in the Shiferaw model), or both after a long period of stimulation at high rates (BCL = 150 ms). In panel A, intracellular calcium and AP are shown for the case when k_{NaCa} is set to the same value as the Chudin model (as was done in the comparisons for this paper) and the sarcolemma pump was active. The resulting intracellular calcium and AP time courses are stationary with respect to time. Panel B shows that decreasing the value of k_{NaCa} from 1177 $\mu A/cm^2$ to 1031 $\mu A/cm^2$ resulted in a higher level of intracellular calcium (although still a low level), but the same stationary behavior in calcium and AP as seen in Panel A. Holding k_{NaCa} = 1177 $\mu A/cm^2$, but disabling the sarcolemma pump had a similar effect. The disabling of the sarcolemma pump and decreasing k_{NaCa} from 1177 $\mu A/cm^2$ to 1031 $\mu A/cm^2$ is shown in Panel C. After 17 s of pacing, the Shiferaw model's intracellular calcium undergoes a series of phenomena that has repeats with a period of 8 s, which includes a 3 s period of unstable oscillations of intracellular calcium, followed by 5 s of periodic calcium alternans. The AP in this same time period exhibits a similar oscillation of APD and amplitude.

4.6. Spontaneous Calcium Release and Myoplasm Calcium in the Chudin Model

In the modified Chudin model, the effect of the reintroduction of spontaneous calcium release was studied in Figure 11. This figure represents the first experiment (paced at BCL = 150 ms) activating spontaneous release in the Chudin model and showing its effect on intracellular calcium and calcium in the JSR when $k_{NaCa} = 2600$ $\mu A/cm^2$ (the value used in the Puglisi-Bers rabbit model). It is evident that the levels of calcium in both the JSR as well as the cytoplasm are relatively low compared to their nominal levels in the guinea pig version of the Chudin model. This results in insufficient

levels of calcium in both the myoplasm and the JSR, leading to no activation of calcium spontaneous release from the JSR.

In order to allow for the appearance of spontaneous calcium release from the JSR, the effects of release thresholds and the sodium calcium exchanger were considered and shown in Figure 12. Results of high pacing rates (BCL = 150 ms), a strong sodium-calcium exchanger (k_{NaCa} = 2000 $\mu A/cm^2$), and modifying the thresholds of spontaneous calcium release from the JSR were considered and each experiment tested the effect of lowering the myoplasm calcium thresholds K_2 and K_4 for spontaneous calcium release from the JSR. In Panel A, no modification to thresholds were done, resulting in small peaks of spontaneous release appearing for the duration of the experiment. Panel B, shows the effect of lowering the lower threshold of myoplasm calcium, K_2, from 0.7 μM to 0.4 μM, which leads to the beginning of quasi-alternans of intracellular calcium after about 5.5 s of pacing in addition to larger peaks of spontaneous calcium release. Lowering both thresholds of myoplasm calcium, K_2 from 0.7 μM to 0.4 μM and K_4 from 1.3 μM to 1.0 μM, shown in Panel C, resulted in even larger peaks of spontaneous calcium release, with residual peaks after stopping stimulation of the model and earlier quasi-alternans of intracellular calcium (~4 s after the beginning of the experiment).

Finally in Figure 13, an analysis similar to that in Figure 12 was done, but with a weak sodium-calcium exchanger (k_{NaCa} = 1177 $\mu A/cm^2$). In Panel A, no modification to thresholds were done, resulting in large, periodic peaks of spontaneous release appearing 3 s after the start of the experiment and leading to quasi-alternans of intracellular calcium with a period of 5 beats. Panel B, shows the effect of lowering the lower threshold of myoplasm calcium, K_2, from 0.7 μM to 0.4 μM, which leads to the beginning of quasi-alternans 3 s after the start of the experiment with a period of 4 beats. More frequent peaks of spontaneous calcium release accompany the resulting quasi alternans of intracellular calcium. Lowering both thresholds of myoplasm calcium, K_2 from 0.7 μM to 0.4 μM and K_4 from 1.3 μM to 1.0 μM, shown in Panel C, resulted in large peaks of spontaneous calcium release earlier than the other two cases and is terminated with several peaks of spontaneous release after the termination of stimulation. Intracellular calcium during the same time period exhibited 5 beat quasi-alternans with a prolongation of the high level of diastolic calcium after the experiment terminated.

5. Conclusion

Comparisons of the guinea pig and rabbit cell models at low and high pacing rates have shown that currents in both models differed significantly in time only in the modifications that Puglisi and Bers introduced, but with differences in AP and intracellular calcium still present. These modifications include the reduction of the fast sodium current, the reduction of the slow delayed rectifier current, and the introduction of two outward (repolarizing) currents: the transient outward potassium current and the calcium activated chlorine current. Figure 4 showed that at high pacing rates, the overall differences in the currents between both models became less pronounced, but alternans in calcium amplitude and APD appeared in the rabbit model, whereas the guinea pig model exhibited steady intracellular calcium accumulation and large amounts of calcium release

from the JSR. After the cessation of stimulation, the reactivation of membrane calcium currents triggered a final calcium release event from the JSR leading to the phenomenon of the DAD in the rabbit model, which was not observed in the guinea pig model. It is then evident from these investigations that the rabbit model demonstrates more arrhythmic behavior at rates characteristic of VT and is therefore a suitable subject of study in the scope of the larger investigation of the mechanisms of arrhythmia formation.

The results presented above for the modified Chudin and Shiferaw models show that inclusion of the sodium and potassium dynamics from the Puglisi-Bers rabbit model with calcium dynamics from either the Chudin model or the Shiferaw model, alternans like behavior arises in the conditions where calcium extrusion processes are depressed and calcium fluxes from the JSR are increased. This alternans-like phenomenon was observed in the absence of spontaneous calcium release from the JSR in both models, as well as a relatively weak sodium-calcium exchanger (k_{NaCa} = 1177 $\mu A/cm^2$), and the inclusion of a sarcolemmal calcium pump for both models. The effect of membrane current dependence on the higher calcium concentration of the submembrane space formulation in the Shiferaw calcium model was shown in Figures 7 and 9 for low and high pacing rates, showing larger calcium currents in the Shiferaw model. It was also seen in Figure 8 that the Chudin formulation, designed to more accurately model high pacing rate behavior than the LRd model, exhibited higher levels of intracellular calcium at high pacing rates compared to the model with the Shiferaw formulation. Figure 10 showed that alternans is an event driven by the loss of the roles the sarcolemmal calcium pump and the sodium calcium exchanger play in stabilizing the level of intracellular calcium in the Shiferaw model. At the long time of stimulation seen in that figure, APs are driven entirely by the stimulus and the periods of calcium oscillation and instability that interrupt the intervals of calcium alternans correspond to a regeneration of sodium current.

Investigations of the effect of the gating variable P_∞ (in the Chudin formulation of spontaneous calcium release from the JSR) revealed that the appearance and characteristics of quasi-alternans were dependent on myoplasmic calcium thresholds (K_2 and K_4) and the strength of the sodium calcium exchanger. As for the modified Chudin model, Figures 11-13 showed that by decreasing the strength of the sodium-calcium exchanger and lowering the threshold of spontaneous calcium release for myoplasmic calcium results in the appearance of more frequent and larger peaks. This results in the appearance of periodic quasi-alternans similar to the one observed in the guinea pig version of the Chudin model under high pacing rates. These mechanisms and other new phenomenon will be investigated when these cell models are used to simulate cardiac electrophysiological processes in two dimensional and three dimensional tissue.

6. Acknowledgements

This investigation was supported by the National Institutes of Health under
Ruth L. Kirschstein National Research Service Award GM008185 from the National Institutes of General Medical Sciences. We thank Drs. James Weiss and Eugene Chudin for useful discussion and comments. In addition, we also thank Drs. Yohannes Shiferaw, José Puglisi, and Ho Hai Van for their technical advice and comments.

7. References

[1] Luo, C.H. and Rudy, Y. 1991. A model of the ventricular cardiac action potential , depolarization, repolarization, and their interaction. *Circ. Res.* 68: 1501-1526.
[2] Luo, C.H. and Rudy, Y. 1994. A dynamic model of the cardiac ventricular action potential. I. Simulations of ionic currents and concentration changes. *Circ. Res.* 74: 1071-1096.
[3] Viswanathan, P.C., Shaw, R.M., and Rudy, Y. 1999. Effects of I_{Kr} and I_{Ks} heterogeneity on action potential duration and its rate dependence. *Circulation.* 99: 2466-2474.
[4] Shiferaw, Y., Watanabe, M.A., Garfinkel, A., Weiss, J.N., and Karma, A. 2003. Model of intracellular calcium cycling in ventricular myocytes. *Biophys. J.* 85: 3666-3686.
[5] Bers, D.M. 2001. Excitation-Contraction Coupling and Cardiac Contractile Force, Kluwer, Boston.
[6] Puglisi, J.L., Yuan, W., Bassani, J.W.M., and Bers, D.M. 1999. Ca^{2+} influx through Ca^{2+} channels in rabbit ventricular myocytes during action potential clamp: influence of temperature. *Circ. Res.* 85:e-7-e16.
[7] Puglisi, J.L. and Bers, D.M. 2001. LabHEART: an interactive computer model of rabbit ventricular myocyte ion channels and Ca transport. *A m. J. Physiol. Cell Physiol.* 281: C2049-C2060.
[8] Shannon, T.R., Ginsburg, K.S., Bers, D.M. 2000a. Reverse mode of the sarcoplamic reticulum calcium pump and load-dependent cytosolic calcium decline in voltage-clamped cardiac myocytes. *Biophys. J.* 78: 322-333.
[9] Shannon, T.R., Ginsburg, K.S., Bers, D.M. 2000b. Potentiation of fractional sarcoplasmic reticulum calcium release by total and free intra-sarcoplasmic reticulum calcium concentration. *Biophys. J.* 78: 334-343.
[10] Bassani, J.W.M., Yuan, W., and Bers, D.M. 1995. Fractional SR Ca release is regulated by trigger Ca and SR Ca content in cardiac myocytes. *Am. J. Physiol. Cell Physiol.* 268: C1313-C1319.
[11] Niggli, E. 1999. Localized intracellular calcium signaling in muscle: calcium sparks and calcium quarks. *Annu. Rev. Physiol.* 61: 311-335.
[12] Stern, M.D., Song, L.S., Cheng, H., Sham, J.S., Yang, H.T., Boheler, K.R., and Rios, E. 1999. Local control models of cardiac excitation-contraction coupling. A possible role of allosteric interactions between ryanodine receptors. *J Gen. Physiol.* 113: 469-489.
[13] Hodgkin, A.L. and Huxley, A.F. 1952. A quantitative description of membrane currents and its applications to conduction and excitation in nerve. *J. Physiol.* 117: 500-544.
[14] Van, H.H. 2005. Computer simulation of single cell action potential using Puglisi-Bers model of the rabbit ventricular myocyte during normal and high pacing rates. Course term project. Los Angeles, CA: Biomedical Engineering, University of California, Los Angeles.
[15] Chudin, E. 1999. Instability of cardiac excitation wave propagation and intracellular calcium dynamics. Ph.D. dissertation. Los Angles, CA: Biomathematics, University of California, Los Angeles.
[16] Chudin, E., Goldhaber, J., Garfinkel, A., Weiss, J., and Kogan, B. 1999. Intracellular Ca^{2+} dynamics and the stability of ventricular tachycardia. *Biophys. J.* 77: 2930-2941.

Figure Captions

Figure 1.
The morphologies of the APs given by mathematical models for the guinea pig and rabbit myocytes in two frames of time, with a BCL = 1500 ms. In panel A, the full time course of the APs for both models can be seen, with the AP of the guinea pig representation having a peak V_{max} 16% larger than that of the rabbit AP. The AP produced by the rabbit model, however, showed an approximately 19 ms lengthening of APD_{90} over the guinea pig representation. Panel B presents a magnified view of phase 0 of both APs, showing that both have nearly identical rise times (the discrepancy due to the different time courses of the fast sodium current) , but with different V_{max} values.

Figure 2.
Comparisons of currents produced by the guinea pig and rabbit mathematical myocyte models at low pacing rates (BCL = 1500 ms). The six plots given shows the morphologies of the main currents affecting the APs and vice versa of both models, paced at BCL = 1500 ms. The top plot of panel A shows that while both models have similar time courses for the fast sodium current, the rabbit model has a 47% smaller current. In the middle plot of panel A, the sodium-calcium exchanger currents in both models are very similar, with the rabbit model showing a longer net outward current (a prolongation of 25 ms). Calcium currents are compared in the bottom plot of panel A, showing a larger magnitude in both the L-type calcium current and the sarcolemmal calcium pump in the rabbit model as opposed to the guinea pig model. Panel B's top plot gives a comparison of the potassium currents in both models, with the fast delayed rectifier currents having similar morphologies with an ~25 ms delay in the rabbit model. The slow delayed rectifier currents, however, of both models diverge from each other, with the guinea pig model having a significantly higher magnitude. A comparison of the non-specific potassium and sodium currents is presented in the middle plot of panel B, showing a larger potassium and sodium component in the rabbit model as compared to the guinea pig model. New currents introduced in the rabbit model, the transient outward current and the calcium-activated chorine current, are shown in the bottom plot of panel B, which result in the sharp repolarization seen in early Phase 1.

Figure 3.
Time courses of AP and intracellular calcium in the rabbit and guinea pig mathematical models at high pacing rates (BCL = 150 ms). The pacing protocol for both models involved pacing with five initial beats longer than 150 ms in duration, which progressively shortened from 250 ms to 150 ms. This procedure was carried out in order to insure that APs in both models would shorten enough in APD_{90} due to dynamic restitution to allow for stationary AP behavior with respect to time. After about 1 s of pacing, periodic alternans of intracellular calcium amplitude arises in the rabbit model, with large peaks corresponding to shortened APDs and vice versa. The guinea pig model, however, exhibits steady accumulation of intracellular calcium without alternans for the first 4.4 seconds of pacing. After this time period, two large releases of calcium from the JSR to the myoplasm due to spontaneous calcium release are observed, followed by the termination of the pacing protocol with the 30^{th} beat. While the guinea pig model

recovers from its systolic peak to return toward its resting state concentration, the rabbit model exhibits a spontaneous rise of systolic calcium at 5.3 s into the simulation, corresponding to a delayed after-depolarization (DAD) in the AP (indicated by the downward arrows).

Figure 4.
Comparisons of currents produced by the guinea pig and rabbit models at high pacing rates (BCL = 150 ms). The six plots given show the effects of fast stimulation rates on several currents in the two models, with all currents measured in the 30^{th} and final beat. The top plot of panel A displays traces for the fast sodium current for the models, with the current in the rabbit model having decreased faster than the one in the guinea pig model. In the middle plot of panel A, the difference in the durations of the outward current phase of the sodium-calcium exchanger between both models has largely disappeared. The plot of calcium currents, shown in the bottom plot of panel A, shows a reduction of discrepancies in magnitudes of the L-type calcium currents in both models and nearly identical traces of the sarcolemmal calcium pump. In Panel B's top plot, a comparison of the potassium currents in both models is given and it can be seen that there is almost a complete disappearance of the discrepancy in time delay of the rapid delayed rectifier current that was seen at slow pacing rates. Also, the slow delayed rectifier current (similar to the rapid delayed rectifier current) shows a shorter time to peak due to dynamic AP restitution at high pacing rates, with a rapid increase at the onset of stimulus application and a smaller difference in current magnitudes midway between their values during low pacing rates. Non-specific potassium and sodium currents are compared in the middle plot of panel B, showing that the amplitudes of both the sodium and potassium currents in both models have increased, with both types of currents larger in the guinea pig model (a reversal of the situation in the low pacing rate regime). The bottom plot of panel B, showing the transient outward potassium and calcium-activated chlorine currents, illustrate little change in the amplitude and time course of the calcium-activated chlorine current, but a 40% decrease in the peak of the transient outward current.

Figure 5.
The dependence of the release function in the Shiferaw model on calcium in the JSR. Presented in this figure is the graphical representation of the release function $Q([Ca^{2+}]_i)$ in the Shiferaw model, plotted against $[Ca^{2+}]_{jsr}$. This is based on the mathematical formulation given in Part II of the Appendix.

Figure 6.
Simulated ventricular action potentials in the modified Chudin and Shiferaw rabbit myocyte models. This figure compares the morphologies of the APs given by mathematical models for the Chudin and Shiferaw rabbit myocytes in two frames of time, with a BCL = 1500 ms. In panel A, the full time course of the APs for both models can be seen, with the APs of both models having nearly identical V_{max} values. The AP produced by the Chudin model, however, showed a more than 40 ms longer APD_{90} than the Shiferaw model. Panel B presents a magnified view of phase 0 of both APs, showing that both have nearly identical rise times and V_{max} values.

Figure 7.
Comparisons of currents produced by the modified Chudin and Shiferaw rabbit myocyte models at low pacing rates. The six plots given shows the morphologies of the main currents affecting the APs and vice versa for both rabbit models, paced at BCL = 1500 ms. The top plot of panel A displays traces for the fast sodium current for the models, both nearly identical to each other. In the middle plot of panel A, the morphologies differ between the two models, with a larger net outward current in the Shiferaw model. Calcium currents are compared in the bottom plot of panel A, showing a nearly four fold increase of L-type calcium current in the Shiferaw model over the Chudin model. The sarcolemmal pump was not actually included in the Shiferaw model, but its trace is shown for completeness. Panel B's top plot gives a comparison of the potassium currents in both models, with the fast delayed rectifier currents having similar morphologies, but different time courses for both models. The slow delayed rectifier currents, however, of both models diverge from each other, with the Chudin model having a significantly higher magnitude. A comparison of the non-specific potassium and sodium currents is presented in the middle plot of panel B, showing that the Shiferaw model has much greater potassium and sodium components in terms of current amplitude. The bottom panel of B displays comparisons of the transient outward potassium and calcium-activated chlorine currents, with the two models having nearly identical transient outward potassium currents, but a divergence in the morphologies of the calcium-activated chlorine currents.

Figure 8.
Time courses of AP and intracellular calcium in the modified Chudin and Shiferaw mathematical models at high pacing rates (BCL = 150 ms). A comparison is made in this figure between the two rabbit models with Chudin and Shiferaw intracellular calcium dynamics and the changes in their characteristics due to high rates of stimulation. As in the earlier comparison of the guinea pig and rabbit models, five initial beats longer than 150 ms in duration paced both AP models from 250 ms to 150 ms gradually in order to attain stationary APs with respect to time. One main feature of the behavior of both models in the high pacing rate regime is that the significant difference in APD_{90} disappears as the dynamic AP restitution properties of both cells shortens the APDs in response to the rate of stimulation. Unlike the case of the guinea pig and rabbit comparison, no alternans in APD is evident in either model. For the plot of intracellular calcium in both models during the same time period, a much higher level of systolic calcium is reached with each successive beat in the modified Chudin model compared to the Shiferaw model. However, no calcium amplitude alternans nor DADs after the cessation of pacing is present in either model in contrast to the presence of both phenomena in the Puglisi-Bers rabbit model.

Figure 9.
Comparisons of currents produced by the modified Chudin and Shiferaw rabbit myocyte models at high pacing rates. The six plots given shows the morphologies of the main currents affecting the APs for both rabbit models, paced at BCL = 150 ms and with all measurements taken at the 30^{th} beat. The top plot of panel A displays traces for the fast sodium current for the models, with the current in the Chudin model nearly zero in contrast to the still significant current from the Shiferaw model. In the middle plot of

panel A, there is a larger net outward in the Shiferaw model, but the differences between the models are less acute than in the case of low pacing rates. Calcium currents are compared in the bottom plot of panel A, showing a greatly reduced discrepancy in magnitudes of the L-type calcium currents in both models. As for the sarcolemmal pump its traces in both models are nearly concise with each other as well. Panel B's top plot gives a comparison of the potassium currents in both models, with a decrease in the differences of the time courses of the fast delayed rectifier currents in both models compared to low pacing rates. The slow delayed rectifier currents, however, still differ greatly in magnitude, with the Chudin model being significantly larger in magnitude than the Shiferaw model at high and low pacing rates. A comparison of the non-specific potassium and sodium currents is presented in the middle plot of panel B, showing that the Shiferaw model has greater potassium and sodium components in terms of current amplitude in high as well as low pacing rates, but less accentuated than at low pacing rates. The bottom panel of B displays comparisons of the transient outward potassium and calcium-activated chlorine currents, with a noticeable decrease in the transient outward current in the Chudin model, but no difference in the calcium-activated chlorine current.

Figure 10.
Effects of the sodium-calcium exchanger and the sarcolemma pump on intracellular calcium and AP in the Shiferaw model. The three plots shown demonstrate the effect of either decreasing the strength of the sodium-calcium exchanger (by decreasing k_{NaCa}), disabling the sarcolemma pump (as was the original condition in the Shiferaw model), or both after a long period of stimulation at high rates (BCL = 150 ms). In panel A, intracellular calcium and AP are shown for the case when k_{NaCa} is set to the same value as the Chudin model (as was done in the comparisons for this paper) and the sarcolemma pump was active. The resulting intracellular calcium and AP time courses are stationary with respect to time. Panel B shows that decreasing the value of k_{NaCa} from 1177 $\mu A/cm^2$ to 1031 $\mu A/cm^2$ resulted in a higher level of intracellular calcium (although still a low level), but the same stationary behavior in calcium and AP as seen in Panel A. Holding k_{NaCa} = 1177 $\mu A/cm^2$, but disabling the sarcolemma pump had a similar effect. The disabling of the sarcolemma pump and decreasing k_{NaCa} from 1177 $\mu A/cm^2$ to 1031 $\mu A/cm^2$ is shown in Panel C. After 17 s of pacing, the Shiferaw model's intracellular calcium undergoes a series of phenomena that has repeats with a period of 8 s, which includes a 3 s period of unstable oscillations of intracellular calcium, followed by 5 s of periodic calcium alternans. The AP in this same time period exhibits a similar oscillation of APD and amplitude.

Figure 11.
Intracellular and JSR calcium at high pacing rates (BCL = 150 ms) with spontaneous release in the modified Chudin model. This figure represents the first experiment activating spontaneous release in the Chudin model and showing its effect on intracellular calcium and calcium in the JSR when k_{NaCa} = 2600 $\mu A/cm^2$ (the value used in the Puglisi-Bers rabbit model). It is evident that the levels of calcium in both the JSR as well as the cytoplasm are relatively low compared to their nominal levels in the guinea pig version of

the Chudin model. This results in insufficient levels of calcium in both the myoplasm and the JSR, leading to no activation of calcium spontaneous release from the JSR.

Figure 12.
Results of high pacing rates (BCL = 150 ms), a strong sodium-calcium exchanger (k_{NaCa} = 2000 $\mu A/cm^2$), and modifying the thresholds of spontaneous calcium release from the JSR for the modified Chudin model. This figure illustrates three sets of experiments in the modified Chudin model where a high coefficient for the sodium-calcium exchanger was used, combined with a high rate of stimulation, where each experiment tested the effect of lowering the myoplasm calcium thresholds K_2 and K_4 for spontaneous calcium release from the JSR. In Panel A, no modification to thresholds were done, resulting in small peaks of spontaneous release appearing for the duration of the experiment. Panel B, shows the effect of lowering the lower threshold of myoplasm calcium, K_2, from 0.7 μM to 0.4 μM, which leads to the beginning of quasi-alternans of intracellular calcium after about 5.5 s of pacing in addition to larger peaks of spontaneous calcium release. Lowering both thresholds of myoplasm calcium, K_2 from 0.7 μM to 0.4 μM and K_4 from 1.3 μM to 1.0 μM, shown in Panel C, resulted in even larger peaks of spontaneous calcium release, with residual peaks after stopping stimulation of the model and earlier quasi-alternans of intracellular calcium (~4 s after the beginning of the experiment).

Figure 13.
Results of high pacing rates (BCL = 150 ms), a weak sodium-calcium exchanger (k_{NaCa} = 1177 $\mu A/cm^2$), and modifying the thresholds of spontaneous calcium release from the JSR for the modified Chudin model. This figure illustrates three sets of experiments in the modified Chudin model where a low coefficient for the sodium-calcium exchanger was used, combined with a high rate of stimulation, where each experiment tested the effect of lowering the myoplasm calcium thresholds K_2 and K_4 for spontaneous calcium release from the JSR. In Panel A, no modification to thresholds were done, resulting in large, periodic peaks of spontaneous release appearing 3 s after the start of the experiment and leading to quasi-alternans of intracellular calcium with a period of 5 beats. Panel B, shows the effect of lowering the lower threshold of myoplasm calcium, K_2, from 0.7 μM to 0.4 μM, which leads to the beginning of quasi-alternans 3 s after the start of the experiment with a period of 4 beats. More frequent peaks of spontaneous calcium release accompany the resulting quasi alternans of intracellular calcium. Lowering both thresholds of myoplasm calcium, K_2 from 0.7 μM to 0.4 μM and K_4 from 1.3 μM to 1.0 μM, shown in Panel C, resulted in large peaks of spontaneous calcium release earlier than the other two cases and is terminated with several peaks of spontaneous release after the termination of stimulation. Intracellular calcium during the same time period exhibited 5 beat quasi-alternans with a prolongation of the high level of diastolic calcium after the experiment terminated.

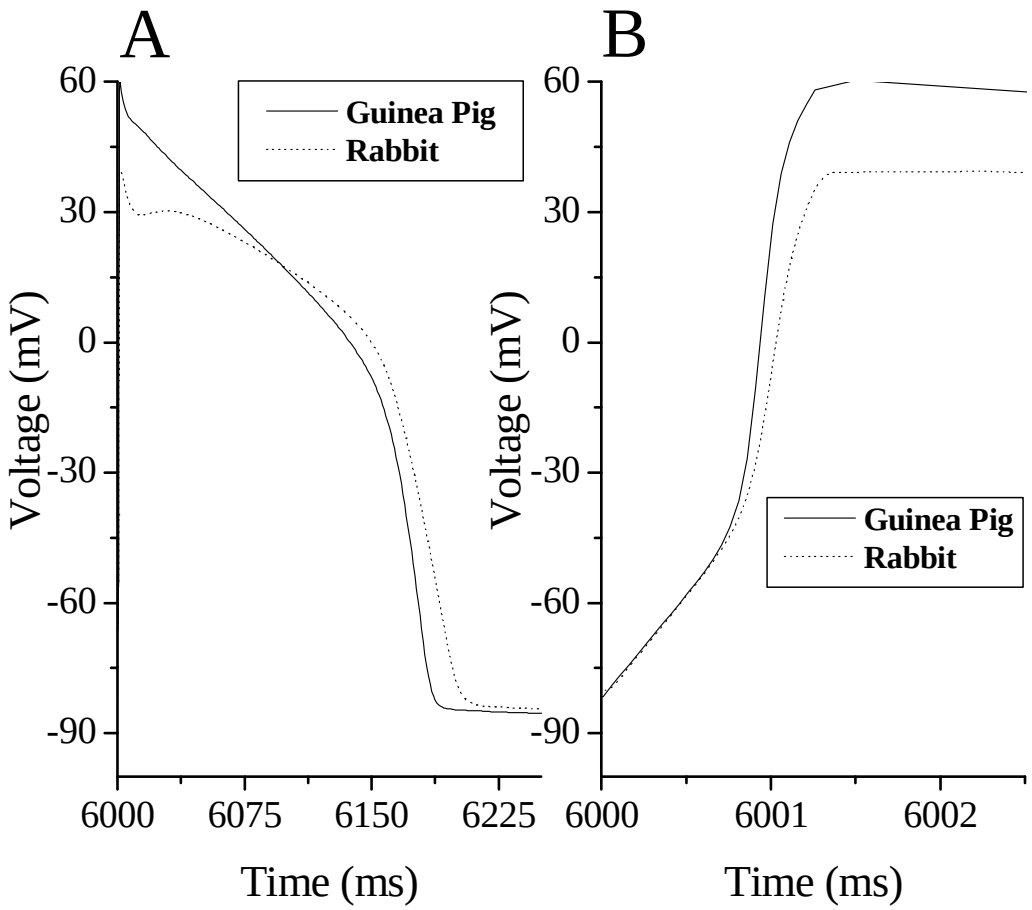
A
B
60
30
0
-30
-60
-90
Voltage (mV)
Guinea Pig
Rabbit
6000
6075
6150
6225
6001
6002
Time (ms)

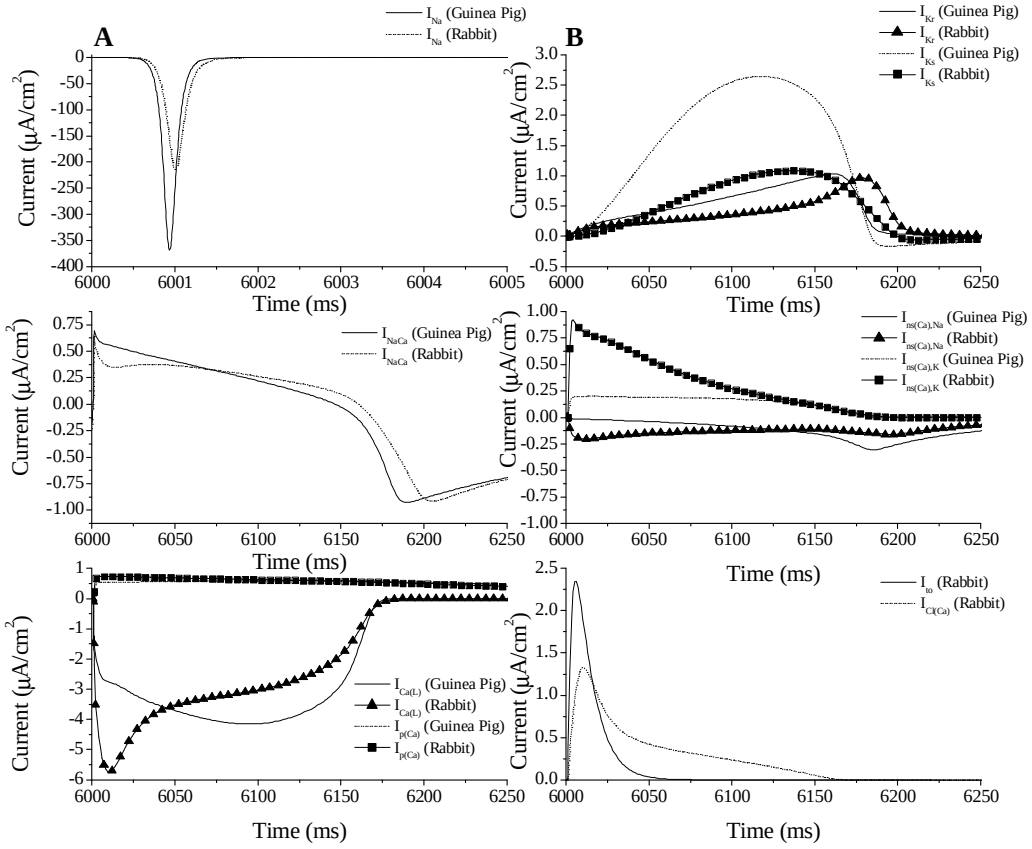
A
B
I_{Na} (Guinea Pig)
I_{Na} (Rabbit)
I_{Kr} (Guinea Pig)
I_{Kr} (Rabbit)
I_{Ks} (Guinea Pig)
I_{Ks} (Rabbit)
I_{NaCa} (Guinea Pig)
I_{NaCa} (Rabbit)
$I_{ns(Ca),Na}$ (Guinea Pig)
$I_{ns(Ca),Na}$ (Rabbit)
$I_{ns(Ca),K}$ (Guinea Pig)
$I_{ns(Ca),K}$ (Rabbit)
$I_{Ca(L)}$ (Guinea Pig)
$I_{Ca(L)}$ (Rabbit)
$I_{p(Ca)}$ (Guinea Pig)
$I_{p(Ca)}$ (Rabbit)
I_{to} (Rabbit)
$I_{Cl(Ca)}$ (Rabbit)
Current (μA/cm^2)
Time (ms)

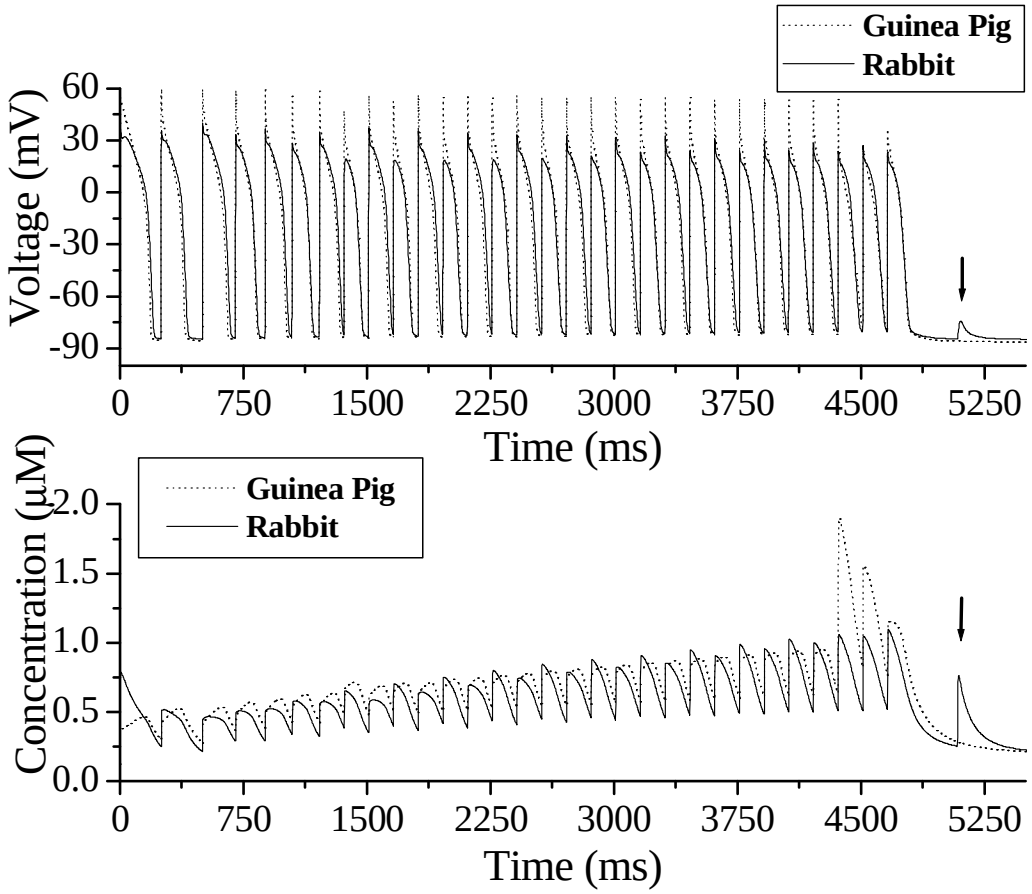
Guinea Pig
Rabbit
Voltage (mV)
60
30
0
-30
-60
-90
0
750
1500
2250
3000
3750
4500
5250
Time (ms)
Guinea Pig
Rabbit
Concentration (μM)
2.0
1.5
1.0
0.5
0.0
0
750
1500
2250
3000
3750
4500
5250
Time (ms)

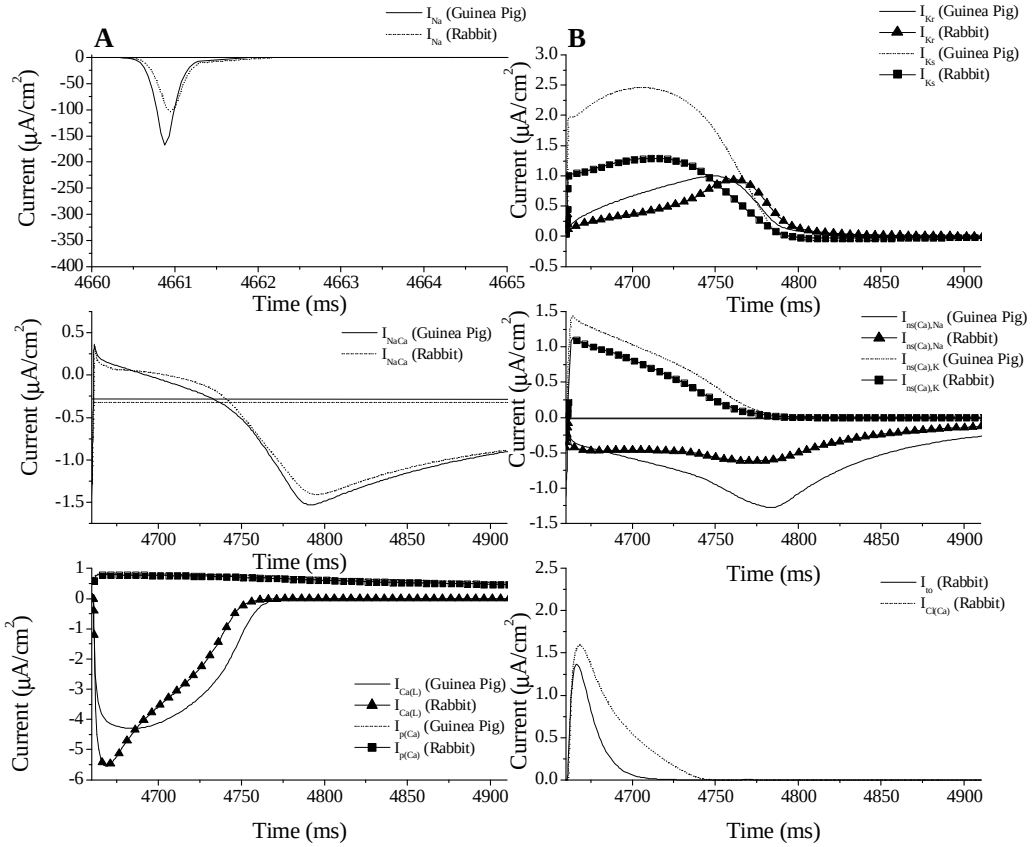
A
B
I_{Na} (Guinea Pig)
I_{Na} (Rabbit)
I_{Kr} (Guinea Pig)
I_{Kr} (Rabbit)
I_{Ks} (Guinea Pig)
I_{Ks} (Rabbit)
I_{NaCa} (Guinea Pig)
I_{NaCa} (Rabbit)
$I_{ns(Ca),Na}$ (Guinea Pig)
$I_{ns(Ca),Na}$ (Rabbit)
$I_{ns(Ca),K}$ (Guinea Pig)
$I_{ns(Ca),K}$ (Rabbit)
$I_{Ca(L)}$ (Guinea Pig)
$I_{Ca(L)}$ (Rabbit)
$I_{p(Ca)}$ (Guinea Pig)
$I_{p(Ca)}$ (Rabbit)
I_{to} (Rabbit)
$I_{Cl(Ca)}$ (Rabbit)
Current (μA/cm^2)
Time (ms)

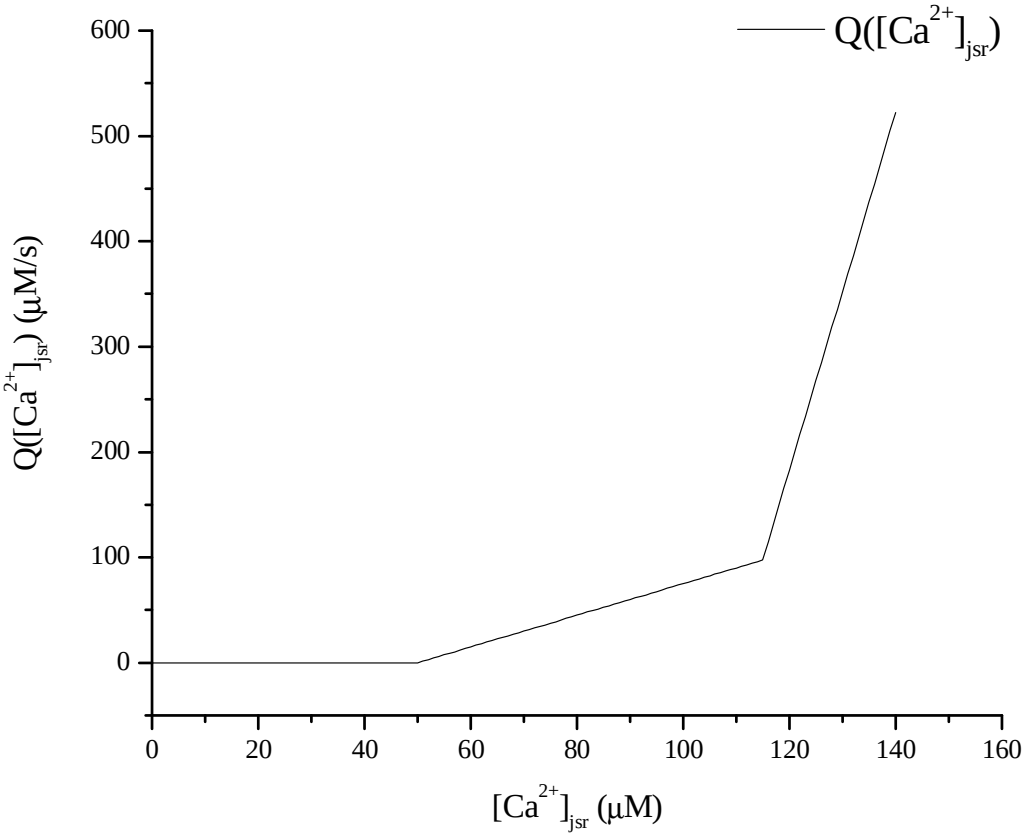
Q([Ca2+]jsr)
600
500
400
300
200
100
0
Q([Ca2+]jsr) (μM/s)
0
20
40
60
80
100
120
140
160
[Ca2+]jsr (μM)

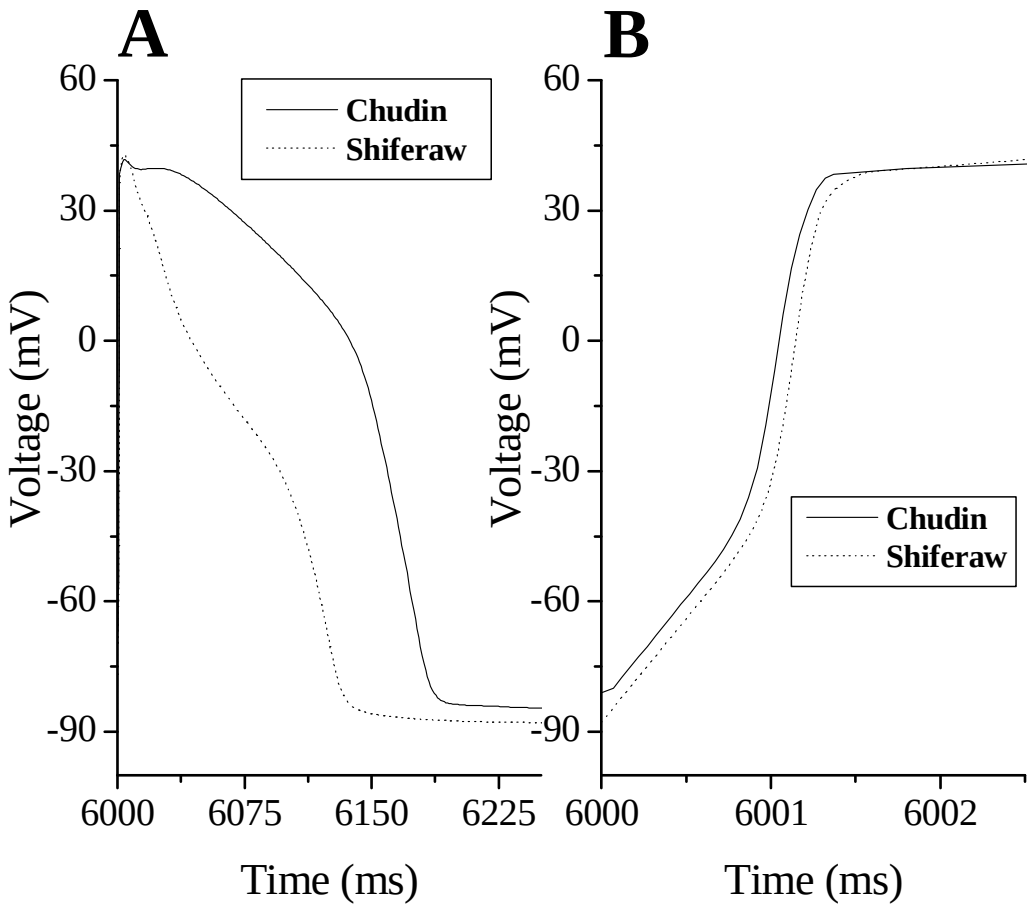
A
B
60
30
0
-30
-60
-90
Voltage (mV)
Chudin
Shiferaw
6000
6075
6150
6225
6001
6002
Time (ms)

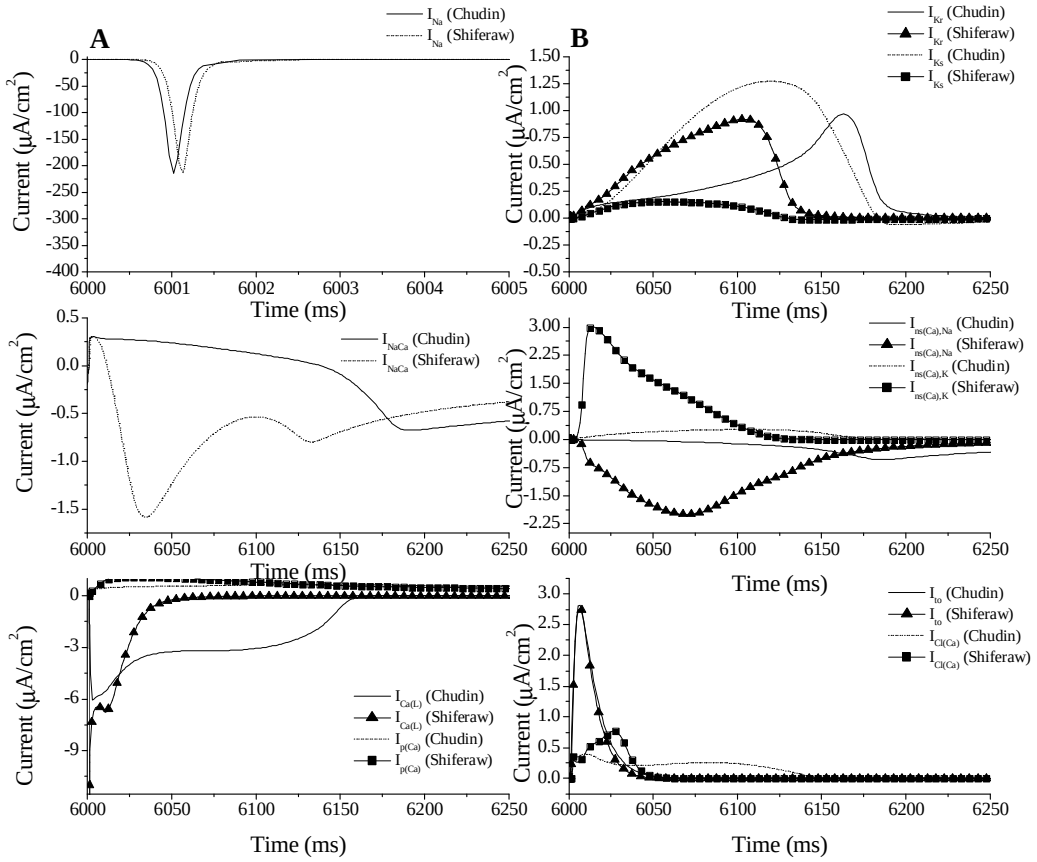
A
B
I_{Na} (Chudin)
I_{Na} (Shiferaw)
I_{Kr} (Chudin)
I_{Kr} (Shiferaw)
I_{Ks} (Chudin)
I_{Ks} (Shiferaw)
I_{NaCa} (Chudin)
I_{NaCa} (Shiferaw)
$I_{ns(Ca),Na}$ (Chudin)
$I_{ns(Ca),Na}$ (Shiferaw)
$I_{ns(Ca),K}$ (Chudin)
$I_{ns(Ca),K}$ (Shiferaw)
$I_{Ca(L)}$ (Chudin)
$I_{Ca(L)}$ (Shiferaw)
$I_{p(Ca)}$ (Chudin)
$I_{p(Ca)}$ (Shiferaw)
I_{to} (Chudin)
I_{to} (Shiferaw)
$I_{Cl(Ca)}$ (Chudin)
$I_{Cl(Ca)}$ (Shiferaw)
Current (μA/cm^2)
Time (ms)

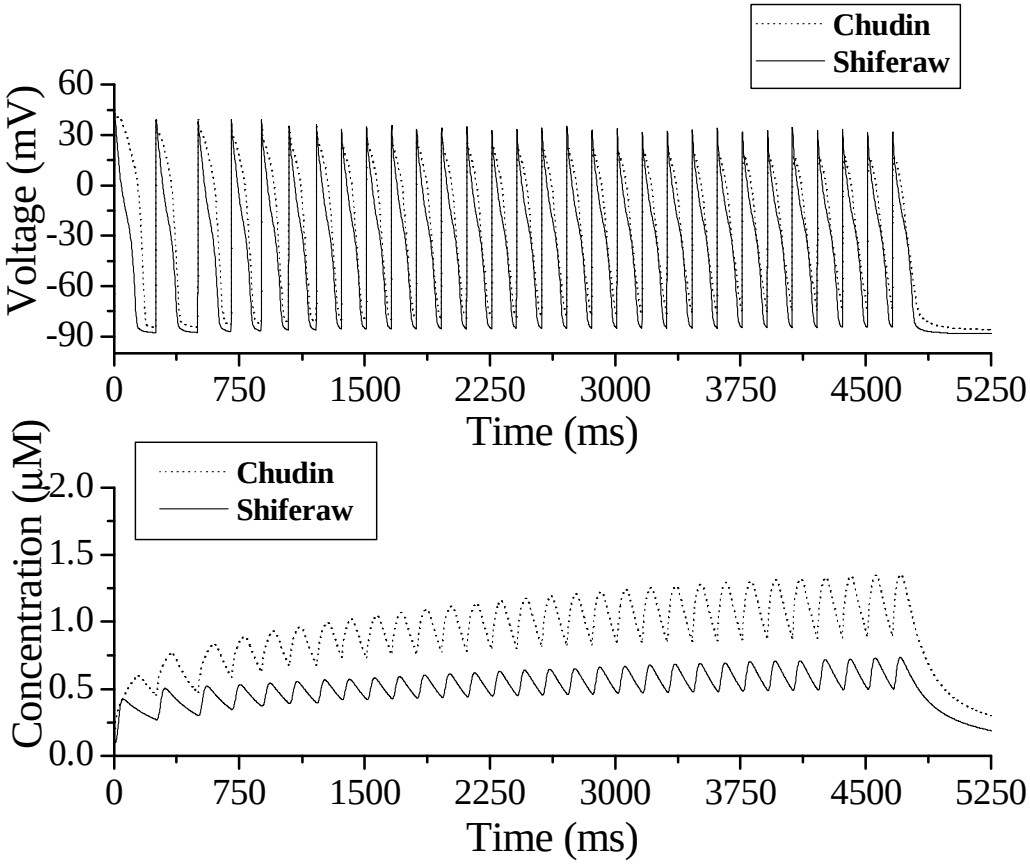
Chudin
Shiferaw
Voltage (mV)
60
30
0
-30
-60
-90
0
750
1500
2250
3000
3750
4500
5250
Time (ms)
Chudin
Shiferaw
Concentration (μM)
2.0
1.5
1.0
0.5
0.0
0
750
1500
2250
3000
3750
4500
5250
Time (ms)

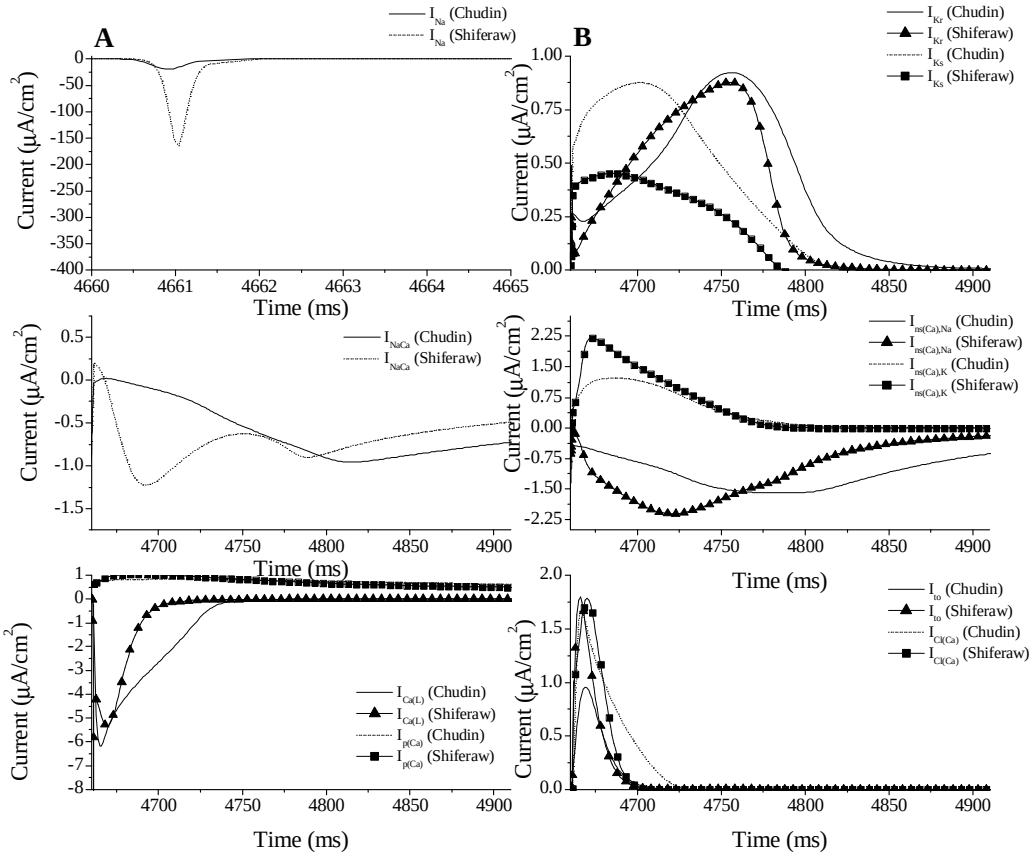
A
B
Current (μA/cm2)
Time (ms)
INa (Chudin)
INa (Shiferaw)
IKr (Chudin)
IKr (Shiferaw)
IKs (Chudin)
IKs (Shiferaw)
INaCa (Chudin)
INaCa (Shiferaw)
Irs(Ca),Na (Chudin)
Irs(Ca),Na (Shiferaw)
Irs(Ca),K (Chudin)
Irs(Ca),K (Shiferaw)
ICa(L) (Chudin)
ICa(L) (Shiferaw)
Ip(Ca) (Chudin)
Ip(Ca) (Shiferaw)
Ito (Chudin)
Ito (Shiferaw)
ICl(Ca) (Chudin)
ICl(Ca) (Shiferaw)

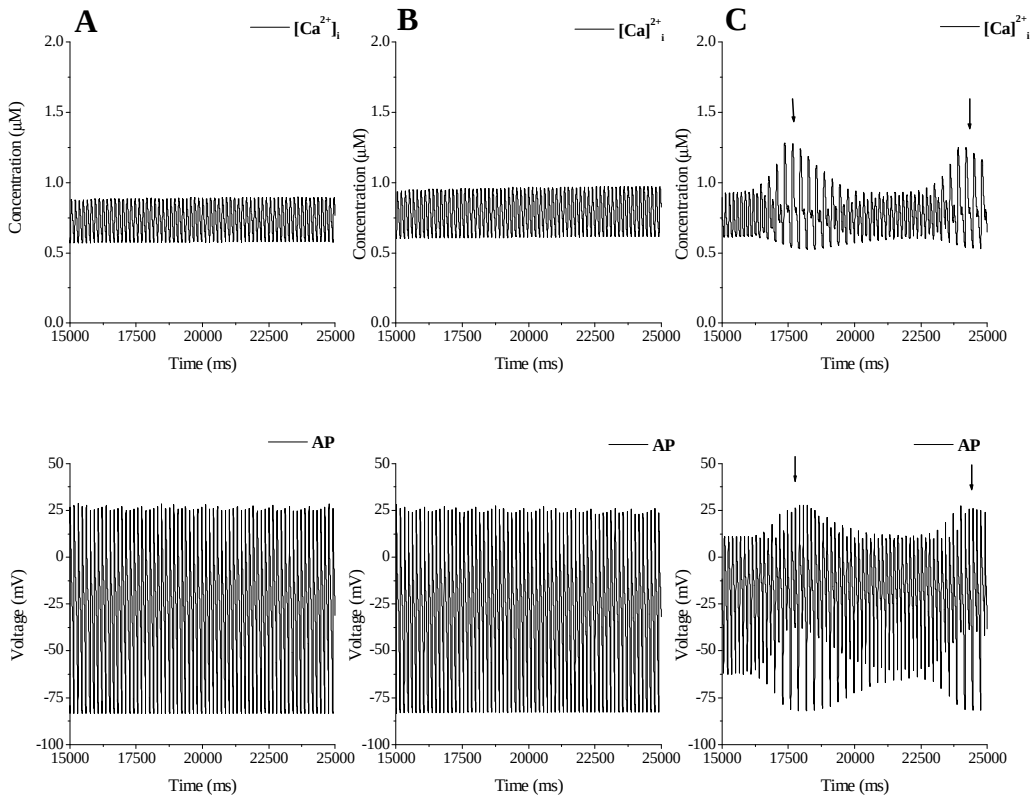
A
B
C
[Ca2+]i
Concentration (μM)
Time (ms)
AP
Voltage (mV)

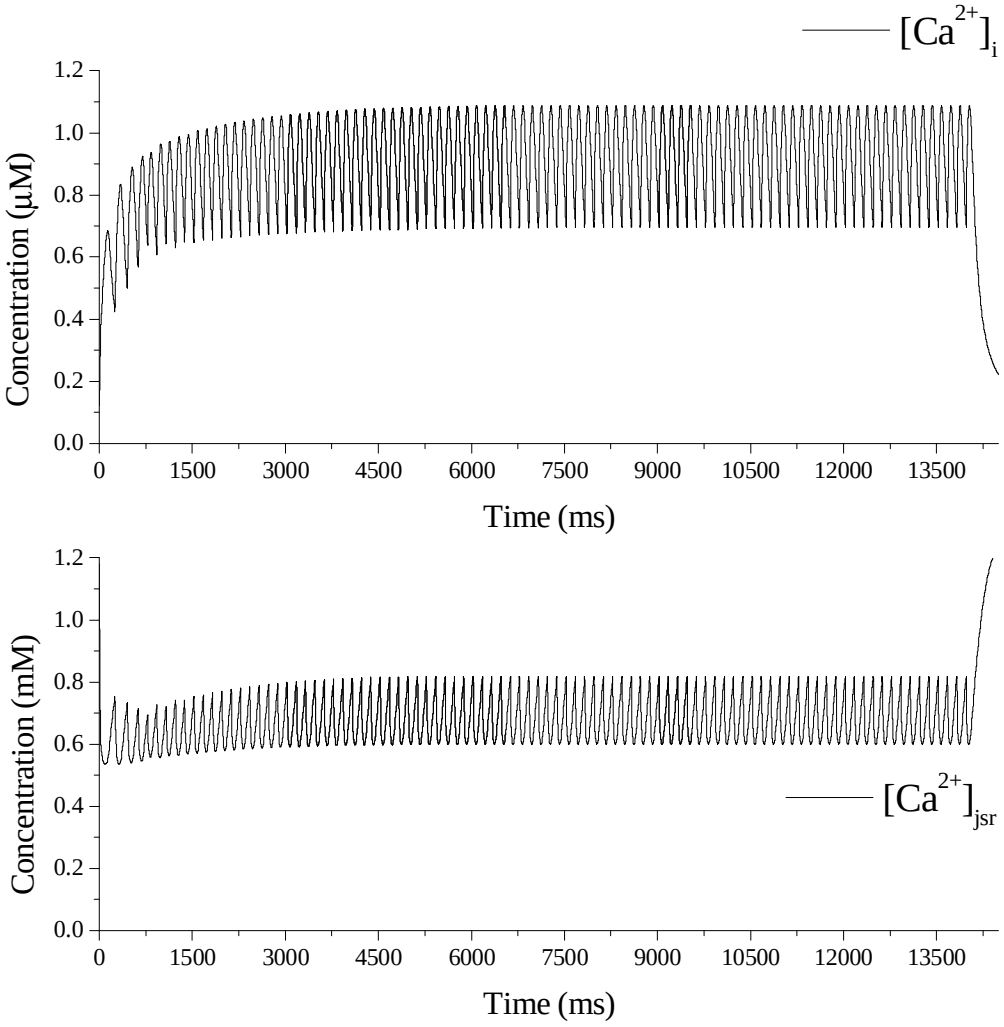
[Ca2+]i
Concentration (μM)
1.2
1.0
0.8
0.6
0.4
0.2
0.0
0
1500
3000
4500
6000
7500
9000
10500
12000
13500
Time (ms)
Concentration (mM)
[Ca2+]jsr
Time (ms)

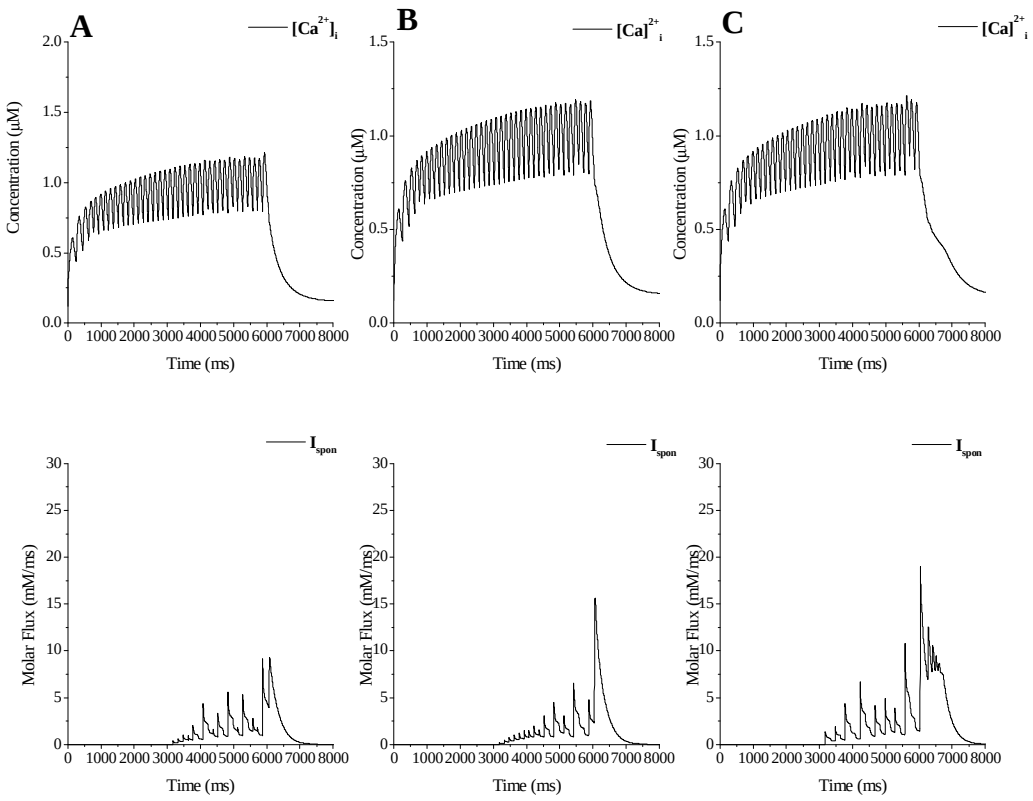
A
B
C
[Ca2+]i
Concentration (μM)
Time (ms)
Ispon
Molar Flux (mM/ms)

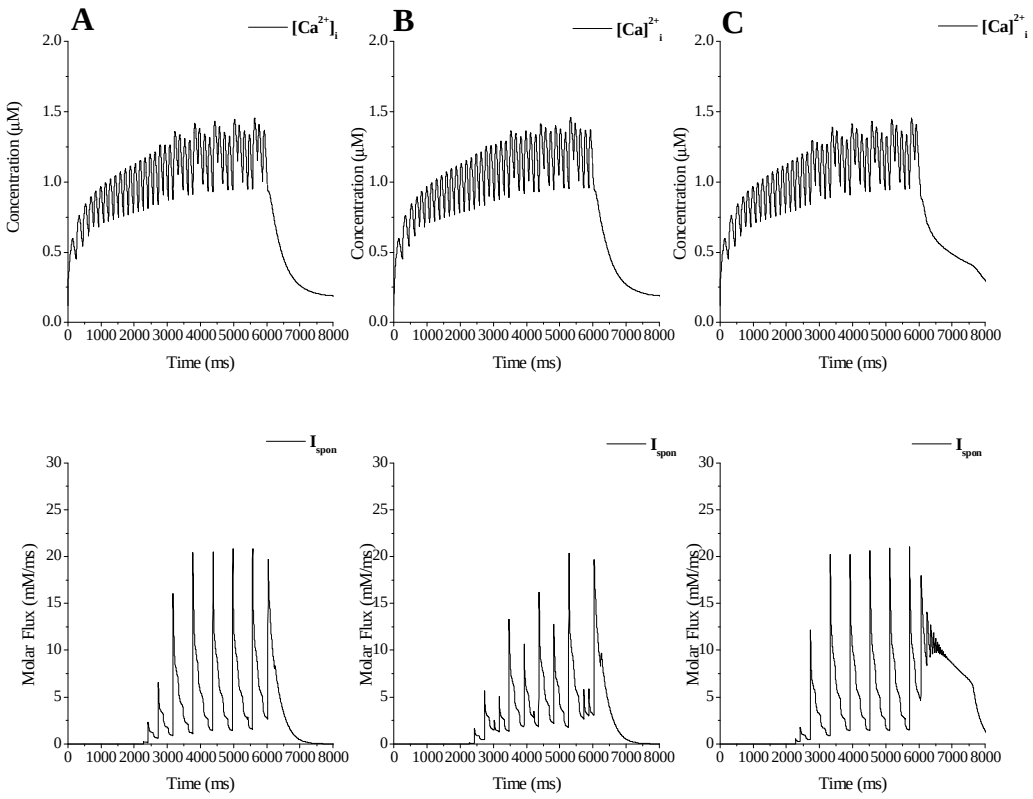
A
B
C
[Ca2+]i
[Ca]2+i
Concentration (μM)
Time (ms)
Ispon
Molar Flux (mM/ms)

Alterations of the Chudin model necessary to produce a mathematical model of the rabbit ventricular myocyte				
Ionic Mechanism	**Symbol**	**Value of Parameter Changed**		**Parameter Changed**
		Guinea Pig	**Rabbit**	
Fast Na^+ current	$\boldsymbol{I_{Na}}$	16.0 $mS/\mu F$	8.0 $mS/\mu F$	G_{Na} reduced by 50%.
Background Na^+ current	$\boldsymbol{I_{Na,b}}$	***N/A***	***N/A***	Same as Chudin.
Non-specific Ca^{2+}-activated Na^+ current	$\boldsymbol{I_{ns(Na)}}$	***N/A***	***N/A***	Same as Chudin.
Na^+- K^+ pump	$\boldsymbol{I_{NaK}}$	***N/A***	***N/A***	Same as Chudin.
Na^+- Ca^{2+} exchanger	$\boldsymbol{I_{NaCa}}$	1177 $\mu A/cm^2$	2600 $\mu A/cm^2$	k_{NaCa} is increased
Rapid delayed rectifier K^+ current	$\boldsymbol{I_{Kr}}$	0.0261 $mS/\mu F$	0.035 $mS/\mu F$	G_{Kr} is increased.
Slow delayed rectifier K^+ current	$\boldsymbol{I_{Ks}}$	See reference	See reference	G_{Ks} reduced by 50%. See reference [7]
Rapid repolarizing K^+ current	$\boldsymbol{I_{K1}}$	0.750 $mS/\mu F$	0.540 $mS/\mu F$	G_{K1} is reduced
Plateau K^+ current	$\boldsymbol{I_{Kp}}$	0.0055 $mS/\mu F$	0.008 $mS/\mu F$	G_{K1} is increased
Transient outward K^+ current	$\boldsymbol{I_{to}}$	See reference	See reference	See reference
Non-specific Ca^{2+}-activated K^+ current	$\boldsymbol{I_{ns(K)}}$	***N/A***	***N/A***	Same as Chudin.
L-type Ca^{2+} current	$\boldsymbol{I_{Ca,L}}$	See reference	See reference	See reference [7]
T-type Ca^{2+} current	$\boldsymbol{I_{Ca,T}}$	See reference	See reference	See reference [7]
Sarcolemmal Ca^{2+} pump	$\boldsymbol{I_{p(Ca)}}$	***N/A***	***N/A***	Same as Chudin.
Background Ca^{2+} current	$\boldsymbol{I_{Ca,b}}$	***N/A***	***N/A***	Same as Chudin.
Ca^{2+}-activated chlorine current	$\boldsymbol{I_{Cl(Ca)}}$	See reference	See reference	See reference [7]
Ca^{2+}-induced Ca^{2+}-release	$\boldsymbol{I_{cicr}}$	See reference	See reference	See reference [15]
Spontaneous Ca^{2+}-release	$\boldsymbol{I_{spon}}$	See reference	See reference	See reference [15]
SR and myoplasm Ca^{2+} buffers	***N/A***	***N/A***	***N/A***	Same as Chudin.

Table 1.
Alterations of the Chudin model necessary to produce a mathematical model of the rabbit ventricular myocyte. In the above table, the first column represents the type of ionic currents, flux, and buffering. The second shows the designation of the mentioned processes above. The remaining columns are: value of the parameter changed, the value for a parameter different between the Chudin and Puglisi-Bers models and the parameter changed, the variable in the expression for the current that was modified. By inspection, it is seen that there is a net increase in the conductances of repolarizing currents, as well as a reduction in I_{Na}, the main depolarizing current. With the addition of $I_{Cl(Ca)}$, I_{to}, and $I_{Ca(T)}$, a net outward (repolarizing) current is introduced, producing the a notch in the AP morphology. It should be noted, however, that for comparison purposes with the Shiferaw based model, the value of the coefficient k_{NaCa} was kept at 1177 $\mu A/cm^2$.

8. Appendix

Part I: Chudin Model [15] with Bers-Puglisi Modifications [7]

- **Cell Geometry**

Length (L) = 157 μm; Radius (r) = 17.27 μm; Geometric Membrane Area (A_{geo}) = $2\pi r^2 + 2\pi rL$ = 1.890×10^{-4} cm^2; Capacitive Membrane Area (A_{cap}) = $2A_{geo}$; Cell Volume (V_{cell}) = $\pi r^2 L = 147.1 \times 10^{-6}$ μL;

Myoplasmic Volume (V_{myo}) = 68%V_{cell} = 100.0×10^{-6} μL;

NSR Volume (V_{nsr}) = 5.52%V_{cell} = 8.120×10^{-6} μL; JSR Volume (V_{jsr}) = 0.48%V_{cell} = 0.706×10^{-6} μL.

- **Standard Ionic Concentrations**

$[K^+]_o$ = 5.4 mM; $[K^+]_i$ = 145 mM; $[Na^+]_o$ = 140 mM; $[Na^+]_i$ = 10 mM; $[Ca^{2+}]_o$ = 1.8 mM.

- **Model Initial Conditions**

v_0 = -85.75130347 mV; m_0 = 0.00136347; j_0 = 0.99187709; d_0 = 0.00000108; f_0 = 0.997928;
b_0 = 0.00204821; g_0 = 0.95223925; $x_{Ks,0}$ = 0.00535361; r_0 = 0.02117561; $x_{to,0}$ = 0.00010155;
$y_{to,0}$ = 0.99999851; p_0 = 0.0; $[Ca^{2+}]_{i,0}$ = 0.12 μM; $[Ca^{2+}]_{jsr,0}$ = 1.179991 mM;
$[Ca^{2+}]_{nsr,0}$ = 1.14885087 mM; $[Ca^{2+}]_{i,cleft,0}$ = 0.000000000175 μM

- **Ionic Currents in the Sarcolemma**

Fast Sodium Current: I_{Na}

$$I_{Na} = \overline{G}_{Na} m^3 hj(V - E_{Na}); \quad E_{Na} = \frac{RT}{F}\ln\left(\frac{[Na^+]_O}{[Na^+]_i}\right); \quad \overline{G}_{Na} = 8.0\frac{mS}{cm^2}$$

$$\alpha_h = \alpha_j = 0; \quad \beta_h = \frac{1.0}{0.13\left[1.0 + \exp\left(-\frac{V + 10.66}{11.1}\right)\right]}; \quad \beta_j = \frac{0.3\exp(-2.535 \cdot 10^{-7} V)}{1.0 + \exp\left(-\frac{V + 32}{10}\right)}$$

when $V \geq 40\ mV$

$$\alpha_h = 0.135\exp\left(-\frac{V + 80}{6.8}\right); \quad \beta_h = 3.56\exp(0.079 \cdot V) + 3.1 \cdot 10^5 \exp(0.35 \cdot V)$$

$$\alpha_j = -(V + 37.78)\frac{1.2714 \cdot 10^5 \exp(0.2444 \cdot V) + 3.474 \cdot 10^{-5} \exp(-0.04391 \cdot V)}{1.0 + \exp(0.311(V + 79.23))}$$

$$\beta_j = \frac{0.1212\exp(-0.01052 \cdot V)}{1.0 + \exp(-0.1378(V + 40.14))}$$

when $V < -40mV$

$$\alpha_m = \frac{0.32(V + 47.13)}{1.0 - \exp(-0.1(V + 47.13))}; \quad \beta_m = 0.08\exp\left(-\frac{V}{11.0}\right) \qquad \forall V$$

Current Through the T-type Channel: $I_{Ca(T)}$

$$I_{Ca(T)} = \overline{G}_{Ca(T)} bg(V - E_{Ca}); \quad \overline{G}_{Ca(T)} = 0.05\frac{mS}{cm^2}; \quad E_{Ca} = \frac{RT}{2F}\ln\left(\frac{\left[Ca^{2+}\right]_O}{\left[Ca^{2+}\right]_i}\right)$$

$$b_\infty = \frac{1.0}{1.0 + \exp\left(-\frac{V + 48.0}{6.1}\right)}; \quad \tau_b = 0.1 + \frac{5.4}{1.0 + \exp\left(\frac{V + 100.0}{33.0}\right)}$$

$$g_\infty = \frac{1.0}{1.0 + \exp\left(\frac{V + 66.0}{6.6}\right)}; \quad \tau_g = 8.0 + \frac{32.0}{1.0 + \exp\frac{V + 65.0}{5.0}}$$

Current Through the L-type Channel: $I_{Ca(L)}$

$$I_{Ca(L)} = I_{Ca,Ca} + I_{Ca,K} + I_{Ca,Na}; \quad For\ ion\ S = \left\{Ca^{2+}, K^+, Na^+\right\}$$

$$I_{Ca,S} = dff_{Ca}\bar{I}_S, \quad where\ f_{Ca} = \frac{K_{m,Ca}}{K_{m,Ca} + \left[Ca^{2+}\right]_i}; \quad K_{m,Ca} = 0.6\mu M$$

$$\bar{I}_S = P_S z_S^2 \frac{VF^2}{RT}\frac{\gamma_{[S]_I}[S]_i \exp(\phi_S) - \gamma_{[S]_O}[S]_O}{\exp(\phi_S) - 1}, \quad where\ \phi_S = \frac{z_S VF}{RT}$$

$$P_{Ca} = 5.4 \cdot 10^{-4}\frac{cm}{\sec}; \quad \gamma_{[Ca]_I} = 1.0; \quad \gamma_{[Ca]_O} = 0.341$$

$$P_K = 6.75 \cdot 10^{-7}\frac{cm}{\sec}; \quad \gamma_{[K]_I} = 0.75; \quad \gamma_{[K]_O} = 0.75$$

$$P_{Ca} = 1.93 \cdot 10^{-7}\frac{cm}{\sec}; \quad \gamma_{[Na]_I} = 0.75; \quad \gamma_{[Na]_O} = 0.75$$

$$d_\infty = \frac{1.0}{1.0 + \exp\left(-\frac{V}{6.24}\right)}; \quad \tau_d = d_\infty \frac{1 - \exp\left(-\frac{V}{6.24}\right)}{0.035 \cdot V}$$

$$f_\infty = \frac{1.0}{1.0 + \exp\left(\frac{V + 35.06}{8.6}\right)} + \frac{0.6}{1.0 + \exp\left(\frac{50.0 - V}{20.0}\right)}; \quad \tau_f = \frac{50.0}{0.985 \cdot \exp(-0.0337 \cdot V^2) + 1.0}$$

Fast Component of the Delayed Rectifier K^+ Current: I_{Kr}

$$I_{Kr} = \overline{G}_{Kr} x_r r_\infty \left(V - E_{Kr}\right);\ \ \overline{G}_{Kr} = 0.035\sqrt{\frac{\left[K^+\right]_O}{5.4}}\,\frac{mS}{cm^2};\ \ E_{Kr} = \frac{RT}{F}\ln\left(\frac{\left[K^+\right]_O}{\left[K^+\right]_i}\right)$$

$$r_\infty = \frac{1}{1+\exp\left(\dfrac{V+33.0}{22.4}\right)};\ \ x_{r\infty} = \frac{1.0}{1.0+\exp\left(-\dfrac{V+57.0}{7.5}\right)}$$

$$\tau_{X_r} = \frac{1.0}{\dfrac{0.00138\cdot V_1}{1.0-\exp\left(-0.123\cdot V_1\right)} + \dfrac{0.00061\cdot V_2}{\exp\left(0.145\cdot V_2\right)-1.0}};\ \ \textit{where } V_1 = V + 14.0;\ \ V_2 = V + 17.0$$

Slow Component of the Delayed Rectifier K^+ Current: I_{Ks}

$$I_{Ks} = \overline{G}_{Ks} x_{Ks}^2 \left(V - E_{Ks}\right);\ \ E_{Ks} = \frac{RT}{F}\ln\left(\frac{\left[K^+\right]_O + P_{Na,K}\left[Na^+\right]_O}{\left[K^+\right]_i + P_{Na,K}\left[Na^+\right]_i}\right);\ \ P_{Na,K} = 0.01833$$

$$\overline{G}_{Ks} = 0.5\cdot\left(0.057 + \frac{0.19}{1.0+\exp\left(\dfrac{pCa-7.2}{0.6}\right)}\right)\frac{mS}{cm^2};\ \ pCa = -\log\left(\left[Ca^{2+}\right]_i\right) + 3.0,\ \textit{with } \left[Ca^{2+}\right]_i \textit{ in mM}$$

$$x_{Ks\infty} = \frac{1.0}{1.0+\exp\left(\dfrac{1.5-V}{16.7}\right)};\ \ \tau_{X_S} = \frac{1.0}{\dfrac{7.19\cdot 10^{-5}\cdot V_1}{1-\exp\left(-0.148\cdot V_1\right)} + \dfrac{1.31\cdot 10^{-4}\cdot V_1}{\exp\left(0.0687\cdot V_1\right)-1.0}};\ \ V_1 = V + 30$$

Time-Independent K^+ Current: I_{K1}

$$I_{K1} = \overline{G}_{K1} K1_\infty \left(V - E_{K1}\right);\ \ E_{K1} = E_{Kr};\ \ \overline{G}_{K1} = 0.540\sqrt{\frac{\left[K^+\right]_O}{5.4}}\,\frac{mS}{cm^2}$$

$$K1_\infty = \frac{\alpha_{K1}}{\alpha_{K1}+\beta_{K1}};\ \ \alpha_{K1} = \frac{1.02}{1.0+\exp\left(0.238\cdot\left(V - E_{K1} - 59.215\right)\right)}$$

$$\beta_{K1} = \frac{0.49124\cdot\exp\left(0.08032\cdot\left(V - E_{K1} + 5.476\right)\right) + \exp\left(0.06175\cdot\left(V - E_{K1} - 594.31\right)\right)}{1.0+\exp\left(-0.5143\cdot\left(V - E_{K1} + 4.753\right)\right)}$$

Plateau K^+ Current: I_{Kp}

$$I_{Kp} = \overline{G}_{Kp} K_p \left(V - E_{Kp}\right);\ \ \overline{G}_{Kp} = 0.008\,\frac{mS}{cm^2};\ \ E_{Kp} = E_{Kr};\ \ K_p = \frac{1.0}{1.0+\exp\left(\dfrac{7.488-V}{5.98}\right)}$$

Na^+-Ca^{2+} Exchanger Current: I_{NaCa}

$$I_{NaCa} = \frac{k_{NaCa}}{K_{m,Na}^3 + \left[Na^+\right]_O^3} \cdot \frac{\exp(\eta\varphi)\left[Na^+\right]_i^3\left[Ca^{2+}\right]_O - \exp\left((\eta-1)\varphi\right)\left[Na^+\right]_O^3\left[Ca^{2+}\right]_i}{\left(K_{m,Ca} + \left[Ca^{2+}\right]_O\right)\left(1.0 + k_{sat}\exp\left((\eta-1)\varphi\right)\right)}$$

$$k_{NaCa} = 2600\frac{uA}{cm^2};\quad K_{m,Na} = 87.5\ mM;\quad K_{m,Ca} = 1.38\ mM;\quad k_{sat} = 0.1;\quad \eta = 0.35;\quad \varphi = \frac{VF}{RT}$$

Na^+-K^+ Pump Current: I_{NaK}

$$I_{NaK} = \frac{\bar{I}_{NaK}\,\bar{f}_{NaK}\left[K^+\right]_O\left[Na^+\right]_i^{1.5}}{\left(K_{m,Nai}^{1.5} + \left[Na^+\right]_i^{1.5}\right)\left(\left[K^+\right]_O + K_{m,Ko}\right)};\quad \bar{I}_{NaK} = 1.5\frac{uA}{cm^2};\quad K_{m,Nai} = 10.0\ mM;\quad K_{m,Ko} = 1.5\ mM$$

$$\bar{f}_{NaK} = \frac{1.0}{1.0 + 0.1245\cdot\exp\left(-\frac{\varphi}{10.0}\right) + 0.0365\cdot\sigma\cdot\exp(-\varphi)};\quad \varphi = \frac{VF}{RT};\quad \sigma = \frac{1.0}{7.0}\left(\exp\left(\frac{\left[Na^+\right]_O}{67.3}\right) - 1.0\right)$$

Nonspecific Ca^{2+} Activated Current: $I_{ns(Ca)}$

$$I_{ns(Ca)} = I_{ns,Na} + I_{ns,K};\quad For\ ion\ S = \left\{K^+, Na^+\right\}$$

$$I_{ns,S} = \frac{\bar{I}_{ns,S}\left[Ca^{2+}\right]_i^3}{K_{m,ns(Ca)}^3 + \left[Ca^{2+}\right]_i^3};\quad K_{m,ns(Ca)} = 1.2\ \mu M$$

$$\bar{I}_{ns,S} = \bar{I}_S,\ where\ \bar{I}_S\ is\ from\ the\ L-type\ channel,\ with\ P_{ns(Ca)} = 1.75\cdot10^{-7}\ \frac{cm}{\sec}$$

Sarcolemmal Ca^{2+} Pump: $I_{p(Ca)}$

T

$$I_{p(Ca)} = \frac{\bar{I}_{p(Ca)}\left[Ca^{2+}\right]_i}{\left[Ca^{2+}\right]_i + K_{m,p(Ca)}};\quad \bar{I}_{p(Ca)} = 1.15\frac{\mu A}{cm^2};\quad K_{m,p(Ca)} = 0.5\ \mu M$$

Ca^{2+} Background Current: $I_{Ca,b}$

$$I_{Ca,b} = \bar{G}_{Ca,b}\left(V - E_{Ca}\right);\quad \bar{G}_{Ca,b} = 0.003016\frac{mS}{cm^2}$$

Na^+ Background Current: $I_{Na,b}$

$$I_{Ca,b} = \bar{G}_{Na,b}\left(V - E_{Na}\right);\quad \bar{G}_{Na,b} = 0.00141\frac{mS}{cm^2}$$

Transient Outward K^+ Current: I_{to}

$$I_{to} = G_{to} X_{to} Y_{to} \left(V - E_{Kr}\right); \quad G_{to} = 0.060 \frac{mS}{cm^2}$$

$$\alpha_{Xto}(V) = 0.04561 \cdot \exp(0.03577 \cdot V); \quad \beta_{Xto}(V) = 0.0989 \cdot \exp(-0.06237 \cdot V)$$

$$\alpha_{Yto}(V) = \frac{0.005415 \cdot \exp\left(-\frac{V + 33.5}{5.0}\right)}{1.0 + 0.051335 \cdot \exp\left(-\frac{V + 33.5}{5.0}\right)}; \quad \beta_{Yto}(V) = \frac{0.005415 \cdot \exp\left(\frac{V + 33.5}{5.0}\right)}{1.0 + 0.051335 \cdot \exp\left(\frac{V + 33.5}{5.0}\right)}$$

Ca^{2+} Activated Cl^- Current: $I_{Cl(Ca)}$

$$I_{Cl(Ca)} = \overline{G}_{Cl} \frac{\left(V - E_{Cl}\right)}{1 + \left(\frac{K_{m,Ca}}{\left[Ca^{2+}\right]_{i,cleft}}\right)^2}; \quad \overline{G}_{Cl} = 10.0 \frac{mS}{cm^2}; \quad K_{m,Ca} = 0.10\ \mu M; \quad E_{Cl} = -40.0\ mV$$

$$\left[Ca^{2+}\right]_{i,cleft} = -\frac{1}{2} df \bar{I}_{Ca} \Lambda_{i,cleft} \Delta t; \quad \Lambda_{i,cleft} = 6.396 \cdot 10^{-6} \frac{\mu M \cdot cm^2}{\mu C}$$

where d, f, and $\bar{I}_{Ca}$ are from the equation for $I_{Ca(L)}$ and Δt is the size of the time step.

- **Ca^{2+} Buffers in the Myoplasm**

$$|TRP| = \overline{|TRP|} \frac{\left[Ca^{2+}\right]_i}{\left[Ca^{2+}\right]_i + K_{m,TRP}}; \quad \overline{|TRP|} = 70.0\ \mu M; \quad K_{m,TRP} = 0.50\ \mu M$$

$$|CMD| = \overline{|CMD|} \frac{\left[Ca^{2+}\right]_i}{\left[Ca^{2+}\right]_i + K_{m,CMD}}; \quad \overline{|CMD|} = 50.0\ \mu M; \quad K_{m,CMD} = 2.38\ \mu M$$

Here $\overline{|TRP|}$ and $\overline{|CMD|}$ are concentrations of buffered troponin and calmodulin respectively. The above expressions allow one to express $\left[Ca^{2+}\right]_i$ as a function of total Ca^{2+} concentration ($\left[Ca^{2+}\right]_t$) in the myoplasm:

$$\left[Ca^{2+}\right]_i = \frac{1000}{3.0}\left(2\sqrt{B^2 - 3C}\cos\left(\frac{a\cos(E)}{3.0}\right) - B\right),\ where:$$

$$B = \overline{|CMD|} + \overline{|TRP|} + K_{m,TRP} + K_{m,CMD} - 0.001\cdot\left[Ca^{2+}\right]_t$$

$$C = K_{m,TRP}K_{m,CMD} + \overline{|TRP|}\cdot K_{m,CMD} + \overline{|CMD|}\cdot K_{m,TRP} - 0.001\cdot\left[Ca^{2+}\right]_t\left(K_{m,TRP} + K_{m,CMD}\right)$$

$$D = -0.001\cdot\left[Ca^{2+}\right]_t K_{m,TRP}K_{m,CMD}$$

$$E = \frac{9BC - 2B^3 - 27D}{2\sqrt{\left(B^2 - 3C\right)^3}}$$

Note that both $\left[Ca^{2+}\right]_i$ and $\left[Ca^{2+}\right]_t$ are measured in μM; therefore, one needs to use a factor of 1000 to make transitions between mM and μM units.

- **Ca^{2+} Fluxes in the Sarcoplasmic Reticulum**

Ca^{2+} Induced - Ca^{2+} Release Current: I_{cicr}

$$I_{cicr} = G_{cicr}P_{open}P_v\left(\chi\left[Ca^{2+}\right]_{jsr} - \left[Ca^{2+}\right]_i\right);\ G_{cicr} = 60.0\ ms^{-1}$$

$$P_{open} = dff_{Ca};\ P_v = \frac{1.0}{1.0 + 1.65\cdot\exp(0.05\cdot V)};\ \chi = \frac{\left[Ca^{2+}\right]_{jsr}^3}{K_{cicr}^3 + \left[Ca^{2+}\right]_{jsr}^3};\ K_{cicr} = 2.0\ mM$$

Here, *d*, *f*, and f_{Ca} are the gating variables of the L-type Ca^{2+} channel, defined previously in the formulation of $I_{Ca(L)}$. **An Important Note: In order to use the above formula, one should convert $\left[Ca^{2+}\right]_i$ to mM.**

Ca^{2+} Release Under Ca^{2+} Overload Conditions: I_{spon}

$$I_{spon} = G_{spon}P_{spon}\left(\left[Ca^{2+}\right]_{jsr} - \left[Ca^{2+}\right]_i\right);\ G_{spon} = 60.0\ ms^{-1}$$

$$\frac{dP_{spon}}{dt} = \frac{P_\infty - P_{spon}}{\tau_p};\ \tau_p = 20.0 + 200.0\cdot\left(1 - P_\infty\right)\ m\sec$$

$$P_\infty = \begin{cases} \dfrac{\left[Ca^{2+}\right]_{jsr} - K_1}{K_3 - K_1},\ if\ \left(\left[Ca^{2+}\right]_{jsr}, \left[Ca^{2+}\right]_i\right) \in I \\ \dfrac{\left[Ca^{2+}\right]_i - K_2}{K_4 - K_2}\dfrac{\left[Ca^{2+}\right]_{jsr} - K_1}{K_3 - K_1},\ if\ \left(\left[Ca^{2+}\right]_{jsr}, \left[Ca^{2+}\right]_i\right) \in II \\ \dfrac{\left[Ca^{2+}\right]_i - K_2}{K_4 - K_2},\ if\ \left(\left[Ca^{2+}\right]_{jsr}, \left[Ca^{2+}\right]_i\right) \in III \end{cases}$$

$$K_1 = 0.8\ mM;\ K_3 = 1.4\ mM;\ K_2 = 0.7\ \mu M;\ K_4 = 1.3\ \mu M$$

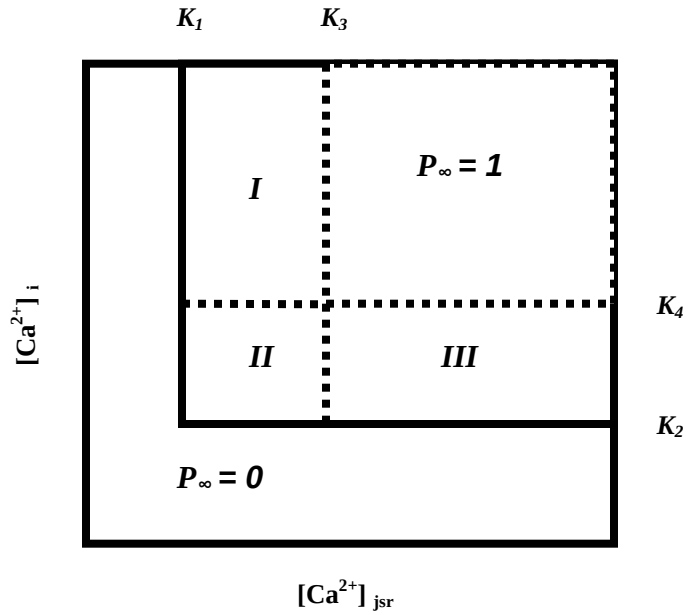

Important Note: To use the formula for I_{spon}, one must convert $\left[Ca^{2+}\right]_i$ to mM.

Ca^{2+} Buffer in the Junctional Sarcoplasmic Reticulum

$$\left|CSQ\right| = \overline{\left|CSQ\right|}\frac{\left[Ca^{2+}\right]_{jsr}}{\left[Ca^{2+}\right]_{jsr} + K_{m,CSQ}};\quad \overline{\left|CSQ\right|} = 10.0\ mM;\quad K_{m,CSQ} = 0.8\ mM$$

Here $\left|CSQ\right|$ is the concentration of buffered calsequestrin. The above expression allows to resolve for free Ca^{2+} in the JSR ($\left[Ca^{2+}\right]_{jsr}$) as a function of total Ca^{2+} concentration ($\left[Ca^{2+}\right]_{t,jsr}$) in the JSR:

$$\left[Ca^{2+}\right]_{jsr} = \frac{1.0}{2.0}\left(b + \sqrt{b^2 + 4\cdot\left[Ca^{2+}\right]_{t,jsr}K_{m,CSQ}}\right);\quad b = \left[Ca^{2+}\right]_{t,jsr} - K_{m,CSQ} - \overline{\left|CSQ\right|}$$

Ca^{2+} Uptake of Network Sarcoplasmic Reticulum: I_{up}

$$I_{up} = \bar{I}_{up}\frac{\left[Ca^{2+}\right]_i^2}{\left[Ca^{2+}\right]_i^2 + K_{m,up}^2}\frac{mM}{m\sec};\quad \bar{I}_{up} = 1.792\cdot 10^{-3}\frac{mM}{m\sec};\quad K_{m,up} = 0.6\ \mu M$$

Ca^{2+} Leak from Network Sarcoplasmic Reticulum: I_{leak}

Important Note: Convert $\left[Ca^{2+}\right]_i$ to mM in order to use the equation below:

$$I_{leak} = g_{leak}\left(\left[Ca^{2+}\right]_{nsr} - \left[Ca^{2+}\right]_i\right);\quad g_{leak} = 1.195\cdot 10^{-4}\ ms^{-1}$$

Ca^{2+} Translocation from the NSR to the JSR: I_{tr}

$$I_{tr} = \frac{\left(\left[Ca^{2+}\right]_{nsr} - \left[Ca^{2+}\right]_{jsr}\right)}{\tau_{tr}} \frac{mM}{m\sec}; \quad \tau_{tr} = 50.0\ m\sec$$

- **Membrane Potential Dynamic**

$$\frac{dV}{dt} = -\frac{1.0}{C}\left(I_{Na} + I_{Ca(T)} + I_{Ca(L)} + I_{Kr} + I_{Ks} + I_{K1} + I_{Kp} + I_{NaCa} + I_{NaK} + I_{ns(Ca)} + I_{p(Ca)} + I_{Ca,b} + I_{Na,b} + I_{to} + I_{Cl(Ca)}\right)$$

Here, $C = 1.0\frac{\mu F}{cm^2}$ is the membrane capacitance per unit area.

- **Dynamics of Gating Variables**

$$\frac{dy}{dt} = \frac{y_\infty(V) - y}{\tau_y(V)}; \quad \tau_y(V) = \frac{1.0}{\alpha_y(V) + \beta_y(V)}; \quad y_\infty(V) = \frac{\alpha_y(V)}{\alpha_y(V) + \beta_y(V)}$$

- **Intracellular Ca^{2+} Dynamics**

$$\frac{d\left[Ca^{2+}\right]_i}{dt} = \left(I_{rel} + I_{spon}\right)\frac{V_{jsr}}{V_{myo}} - \left(I_{Ca(L)} + I_{Ca(T)} + I_{Ca,b} + I_{p(Ca)} - 2I_{NaCa}\right)\frac{A_{cap}}{2V_{myo}F} - \left(I_{up} - I_{leak}\right)\frac{V_{nsr}}{V_{myo}}$$

$$\frac{d\left[Ca^{2+}\right]_{nsr}}{dt} = \left(I_{up} - I_{leak}\right) - I_{tr}\frac{V_{jsr}}{V_{nsr}}$$

$$\frac{d\left[Ca^{2+}\right]_{t,jsr}}{dt} = I_{tr} - I_{rel} - I_{spon}$$

Part II: Shiferaw Model [4] with Bers-Puglisi Modifications [7]

All model parameters are identical to those in the Chudin model except where noted below.

- **Model Initial Conditions**

v_0 = -85.75130347 mV; m_0 = 0.00136347; j_0 = 0.99187709; f_0 = 0.90;
b_0 = 0.00204821; g_0 = 0.95223925; $x_{Ks,0}$ = 0.00535361; r_0 = 0.02117561; $x_{to,0}$ = 0.00010155;
$y_{to,0}$ = 0.99999851; $I_{r,0}$ = 0.0; $[Ca^{2+}]_{i,0}$ = 0.10 μM; $[Ca^{2+}]_{sub,0}$ = 0.10 μM; $[Ca^{2+}]_{jsr,0}$ = 0.110 μM;
$[Ca^{2+}]_{sr,0}$ = 0.110 μM; $[Ca^{2+}]_{t,i,0}$ = 10.0 μM; $[Ca^{2+}]_{t,sub,0}$ = 10.0 μM; $[Ca^{2+}]_{i,cleft,0}$ = 0.000000000175 μM

Current Through the T-type Channel: $I_{Ca(T)}$

This current is omitted in the Shiferaw model.

Current Through the L-type Channel: $I_{Ca(L)}$

$$I_{Ca(L)} = I_{Ca,Ca} + I_{Ca,K} + I_{Ca,Na};\ \ For\ ion\ S = \left\{Ca^{2+}, K^{+}, Na^{+}\right\}$$

$$I_{Ca,S} = d_{\infty}\, ff_{Ca}\, \bar{I}_S,\ \ where\ f_{Ca(\infty)} = \frac{1.0}{1.0 + \dfrac{\left[Ca^{2+}\right]_{sub}}{K_{m,Ca}}};\ \ \tau_{Ca(\infty)} = \frac{f_{Ca(\infty)}}{k_O};\ \ k_O = 8s^{-1};\ \ K_{m,Ca} = 0.5\mu M$$

$$\bar{I}_S = P_S z_S^2 \frac{VF^2}{RT} \frac{\gamma_{[S]_I}[S]_i \exp\left(\phi_S\right) - \gamma_{[S]_O}[S]_O}{\exp\left(\phi_S\right) - 1},\ \ where\ \phi_S = \frac{z_S VF}{RT}$$

$$P_{Ca} = 5.4 \cdot 10^{-4}\ \frac{cm}{\sec};\ \ \gamma_{[Ca]_I} = 1.0;\ \ \gamma_{[Ca]_O} = 0.341;\ \ [S]_i = \left[Ca^{2+}\right]_{sub}\ for\ Ca^{2+}$$

$$P_K = 6.75 \cdot 10^{-7}\ \frac{cm}{\sec};\ \ \gamma_{[K]_I} = 0.75;\ \ \gamma_{[K]_O} = 0.75$$

$$P_{Ca} = 1.93 \cdot 10^{-7}\ \frac{cm}{\sec};\ \ \gamma_{[Na]_I} = 0.75;\ \ \gamma_{[Na]_O} = 0.75$$

$$d_{\infty} = \frac{1.0}{1.0 + \exp\left(-\dfrac{(V - 5.0)}{6.24}\right)};\ \ \tau_d\ is\ not\ applicable.$$

$$f_{\infty} = \frac{1.0}{1.0 + \exp\left(\dfrac{V + 35.06}{8.6}\right)};\ \ \tau_f = 30\ ms^{-1}$$

Slow Delayed Rectifier K^+ Current: I_{Ks}

pCa is dependent on the concentration of calcium in the submembrane space instead of $[Ca^{2+}]_i$.

Na^+-Ca^{2+} Exchanger Current: I_{NaCa}

$$I_{NaCa} = \frac{k_{NaCa}}{K_{m,Na}^3 + \left[Na^{+}\right]_O^3} \cdot \frac{\exp\left(\eta\varphi\right)\left[Na^{+}\right]_i^3\left[Ca^{2+}\right]_O - \exp\left((\eta - 1)\varphi\right)\left[Na^{+}\right]_O^3\left[Ca^{2+}\right]_{sub}}{\left(K_{m,Ca} + \left[Ca^{2+}\right]_O\right)\left(1.0 + k_{sat}\exp\left((\eta - 1)\varphi\right)\right)}$$

$$k_{NaCa} = 1021\frac{uA}{cm^2};\ \ K_{m,Na} = 87.5\ mM;\ \ K_{m,Ca} = 1.38\ mM;\ \ k_{sat} = 0.1;\ \ \eta = 0.35;\ \ \varphi = \frac{VF}{RT}$$

Nonspecific Ca^{2+} Activated Current: $I_{ns(Ca)}$

$I_{ns,S}$ is dependent on the concentration of calcium in the submembrane space instead of $[Ca^{2+}]_i$.

Sarcolemmal Ca^{2+} Pump: $I_{p(Ca)}$

This current is omitted in the Shiferaw model.

Ca^{2+} Background Current: $I_{Ca,b}$

This current is omitted in the Shiferaw model.

Ca^{2+} Activated Cl^- Current: $I_{Cl(Ca)}$

$[Ca^{2+}]_{i,cleft}$ is dependent on the concentration of calcium in the submembrane space instead of $[Ca^{2+}]_i$.

- **Ca^{2+} Buffers in the Myoplasm and the Sub-membrane Space**

Buffering dynamics reformulated, see the description of calcium time-dependent dynamics below.

- **Ca^{2+} Fluxes in the Sarcoplasmic Reticulum**

Ca^{2+} Current Draining the Sarcoplasmic Reticulum: I_r

This release flux from the SR substitutes for I_{cicr} in the Chudin model.

$$\frac{dI_r}{dt} = gI_{Ca(L)}Q\left(c_j'\right) - \frac{I_r}{\tau_r};\ \ g = 37.5\cdot 10^4\,\frac{sparks}{C};\ \ \tau_r = 20\ ms^{-1}$$

$$Q\left(c_j'\right) = \begin{cases} 0, & 0 < c_j' < 50\ \mu M \\ 1.5\cdot\left(c_j' - 50.0\right)\dfrac{\mu M}{s}, & 50\ \mu M \le c_j' < 115\ \mu M; \\ \left(uc_j' + s\right)\dfrac{\mu M}{s}, & c_j' \ge 115\ \mu M \end{cases}$$

$$u = 11.3\ s^{-1};\ \ s = 1.5\cdot(115.0 - 50.0) - u\cdot 115.0\,\frac{\mu M}{s}$$

Here, c_j' is the Ca^{2+} concentration in the JSR.

Ca^{2+} Release Under Ca^{2+} Overload Conditions: I_{spon} *(CHANGES PRESENT)*

This flux is omitted in the Shiferaw model.

Ca^{2+} Buffer in the Junctional Sarcoplasmic Reticulum

Buffering dynamics reformulated, see the description of calcium time-dependent dynamics below.

Ca^{2+} Leak from Network Sarcoplasmic Reticulum: I_{leak}

This flux is omitted in the Shiferaw model.

Ca^{2+} Translocation from the NSR to the JSR: I_{tr} *(CHANGES PRESENT)*

I_{tr} is dependent on the average SR concentration instead of $[Ca^{2+}]_{nsr}$.

Ca^{2+} Flux to Troponin in the Myoplasm and Sub-membrane Space: I_{trpn}^{S}

$$\frac{d[CaT]_S}{dt} = I_{trpn}^{S} = k_{on}^{T}\left[Ca^{2+}\right]_S\left(B_T - [CaT]_S\right) - k_{off}^{T}[CaT]_S$$

$$k_{on}^{T} = 32.7\frac{1.0}{\mu M \cdot s};\ \ k_{off}^{T} = 19.6\ s^{-1};\ \ B_T = 70\frac{\mu mol}{L\ cytosol};\ \ S = \{i,\ sub\}$$

Ca^{2+} Buffering to Calmodulin and SR Membrane Binding Sites in the Myoplasm and Sub-membrane Space:

$$\beta\left(\left[Ca^{2+}\right]_S\right) = \left[1.0 + \frac{B_{SR}K_{SR}}{\left(\left[Ca^{2+}\right]_S + K_{SR}\right)^2} + \frac{B_{Cd}K_{Cd}}{\left(\left[Ca^{2+}\right]_S + K_{Cd}\right)^2}\right]^{-1};\ \ S = \{i,\ sub\}$$

$$B_{SR} = 47.0\frac{\mu mol}{Lcytosol};\ \ B_{Cd} = 24.0\frac{\mu mol}{Lcytosol};\ \ K_{SR} = 0.6\ \mu M;\ \ K_{Cd} = 7.0\ \mu M$$

- **Intracellular Ca^{2+} Dynamics**

$$\frac{d\left[Ca^{2+}\right]_{sub}}{dt} = \beta\left(\left[Ca^{2+}\right]_{sub}\right)\left[\frac{v_i}{v_{sub}}\left(I_r - \frac{\left[Ca^{2+}\right]_{sub} - \left[Ca^{2+}\right]_i}{\tau_{sub}} - I_{Ca(L)} + I_{NaCa}\right) - I_{trpn}^{sub}\right]$$

$$\frac{d\left[Ca^{2+}\right]_i}{dt} = \beta\left(\left[Ca^{2+}\right]_i\right)\left(\frac{\left[Ca^{2+}\right]_{sub} - \left[Ca^{2+}\right]_i}{\tau_{sub}} - I_{up} - I_{trpn}^{i}\right)$$

$$\frac{d\left[Ca^{2+}\right]_{sr}}{dt} = -I_r + I_{up}$$

$$\frac{d\left[Ca^{2+}\right]_{t,jsr}}{dt} = I_{tr}$$

$$\frac{v_i}{v_{sub}} = 10.0;\ \ \tau_{sub} = 10\ ms^{-1}$$